

Helicity Evolution at Small x

Yuri V. Kovchegov*

Department of Physics, The Ohio State University, Columbus, OH 43210, USA

Daniel Pitonyak†

RIKEN BNL Research Center, Brookhaven National Laboratory, Upton, New York 11973, USA

Matthew D. Sievert‡

Physics Department, Brookhaven National Laboratory, Upton, NY 11973, USA

We construct small- x evolution equations which can be used to calculate quark and anti-quark helicity TMDs and PDFs, along with the g_1 structure function. These evolution equations resum powers of $\alpha_s \ln^2(1/x)$ in the polarization-dependent evolution along with the powers of $\alpha_s \ln(1/x)$ in the unpolarized evolution which includes saturation effects. The equations are written in an operator form in terms of polarization-dependent Wilson line-like operators. While the equations do not close in general, they become closed and self-contained systems of non-linear equations in the large- N_c and large- N_c & N_f limits. As a cross-check, in the ladder approximation, our equations map onto the same ladder limit of the infrared evolution equations for the g_1 structure function derived previously by Bartels, Ermolaev and Ryskin [1].

PACS numbers: 12.38.-t, 12.38.Bx, 12.38.Cy

I. INTRODUCTION

Our understanding of high-energy quantum chromodynamics (QCD) has expanded greatly in the past two decades, in part due to the new and exciting developments in saturation physics [2–9] and non-linear small- x evolution [10–20] (see [2, 21–26] for reviews and a book). During those developments, most of the research effort was dedicated to calculating unpolarized observables, such as total cross sections, unpolarized particle production and correlations. In more recent years the interest in applying the formalism of small- x physics to calculating polarization-dependent observables has been on the rise [27–46], with particular attention being devoted to calculating the quark and gluon transverse momentum-dependent parton distribution functions (TMDs) of the proton [47, 48]. The goal of the present work is to apply the small- x saturation formalism to helicity evolution in order to assess the amount of proton’s spin carried by the partons at small x .

One of the most profound mysteries in our understanding of the proton structure is the so-called spin puzzle [49, 50] (see [51–53] for a comprehensive review of the experimental situation and additional references): the presently measured spin and orbital angular momentum (OAM) carried by the quarks and gluons inside the proton does not appear to add up to 1/2. The puzzle can be formalized in terms of helicity sum rules [54–56] such as the Jaffe-Manohar form [54]

$$S_q + L_q + S_G + L_G = \frac{1}{2}. \quad (1)$$

Here L_q and L_G are the orbital angular momenta of the quarks and gluons respectively, while S_q and S_G denote the spin carried by all the quarks and gluons and are defined as the following integrals over Bjorken- x at fixed momentum scale Q^2

$$S_q(Q^2) = \frac{1}{2} \int_0^1 dx \Delta\Sigma(x, Q^2), \quad S_G(Q^2) = \int_0^1 dx \Delta G(x, Q^2) \quad (2)$$

with

$$\Delta\Sigma(x, Q^2) = [\Delta u + \Delta\bar{u} + \Delta d + \Delta\bar{d} + \dots](x, Q^2), \quad (3)$$

* Email: kovchegov.1@osu.edu

† Email: dpitonyak@quark.phy.bnl.gov

‡ Email: msievert@bnl.gov

and the helicity parton distribution functions (hPDFs)

$$\Delta f(x, Q^2) \equiv f^+(x, Q^2) - f^-(x, Q^2). \quad (4)$$

In (4) f^+ (f^-) denote the number density of partons with the same (opposite) helicity as the proton, and $f = u, \bar{u}, d, \bar{d}, \dots, G$.

Indeed in the actual experiments due to finite center-of-mass energy one cannot measure $\Delta\Sigma$ and ΔG down to $x = 0$ as required by Eq. (2): these quantities are measured down to some minimal available value of x instead. The current quark and gluon spin values extracted from the experimental data are $S_q(Q^2 = 10 \text{ GeV}^2) \approx 0.15 \div 0.20$ (integrated over $0.001 < x < 1$) and $S_G(Q^2 = 10 \text{ GeV}^2) \approx 0.13 \div 0.26$ (integrated over $0.05 < x < 1$) [57–59]. Even the largest values of S_q and S_G (in the above ranges) do not add up to give 1/2. The missing proton’s spin is likely to be in the quark and gluon OAM and/or at smaller values of x . It is, therefore, important to gain good qualitative and quantitative understanding of the behavior of $\Delta\Sigma$ and ΔG at small x . A strong growth of these quantities at small x may indicate that a large amount of proton spin resides in that region of phase space, possibly offering a solution to the proton spin puzzle.

The small- x evolution of the quark polarization and flavor-dependent observables was first considered by Kirschner and Lipatov in [60] (see also [61–63]). The calculation was similar to the well-known Balitsky–Fadin–Kuraev–Lipatov (BFKL) equation [64, 65], using quarks instead of gluons as the t -channel lines in the corresponding ladder. In addition, non-ladder diagrams turned out to be important in the calculation, making it very hard to resum all the relevant graphs using the BFKL-like evolution equation in rapidity; the resummation in [60] was instead performed using a (non-linear) evolution in the infrared cutoff. Perhaps most importantly it was demonstrated that the small- x limit of the quark-exchange amplitudes is dominated by the resummation of the double-logarithmic (DLA) parameter $\alpha_s \ln^2 s \sim \alpha_s \ln^2(1/x)$ (with s the center of mass energy squared and α_s the strong coupling constant).¹ This is in contrast to the standard BFKL evolution, along with the nonlinear Balitsky–Kovchegov (BK) [13–16] and Jalilian-Marian–Iancu–McLerran–Weigert–Leonidov–Kovner (JIMWLK) [17–20] evolution equations, all of which, at the leading order in α_s in the kernel resum powers of single logarithm, $\alpha_s \ln(1/x)$. For the $\alpha_s \ln^2(1/x)$ parameter to become important one does not need x to be as small as would be needed for the $\alpha_s \ln(1/x)$ parameter to become important: hence the effects of small- x evolution on polarization-dependent observables may be stronger and easier to observe in experiments than the small- x evolution for unpolarized observables.

The small- x limit of an observable relevant to the spin puzzle, the structure function $g_1(x, Q^2)$, was first considered by Bartels, Ermolaev and Ryskin (from now on referred to as BER) in [1, 66]. At the leading order in α_s and at leading twist this structure function is

$$g_1(x, Q^2) = \frac{1}{2} \sum_{f=\text{quarks}} Z_f^2 [\Delta f(x, Q^2) + \Delta \bar{f}(x, Q^2)] \quad (5)$$

with Z_f the electric charge of a quark of flavor f in units of the electron’s charge. Resumming double-logarithms $\alpha_s \ln^2(1/x)$ using the infrared evolution equations, BER obtained a tantalizing result: they argued that at small x the $g_1(x, Q^2)$ structure function, and, hence $\Delta\Sigma$, grow as $(1/x)^{\omega_s}$ with a fairly large power $\omega_s = 1.01$ for $\alpha_s = 0.18$ (with presumably larger ω_s for larger values of the coupling α_s). This result appears to indicate that small- x partons may contribute a substantial amount to the net quark (and gluon) spin in the proton S_q (S_G).

The emerging physical picture of the proton would be quite interesting: the majority of small- x partons, generated through BFKL/BK/JIMWLK evolution are unpolarized. Nonetheless, there may exist a minority of small- x partons, generated though the non-eikonal spin-dependent evolution, which carry a potentially large fraction of the proton spin.

Our main aim in this work is to reproduce the results of BER using the s -channel evolution language of [10–20], which employs the light-cone Wilson line operators and, ultimately, color dipoles. Moreover, we want to include saturation corrections into the evolution equations, thus going beyond the evolution considered by BER. Indeed saturation corrections resum single logarithms and strictly speaking should come in only at the level of the next-to-leading order (NLO) corrections to the DLA helicity evolution. However, in the cases considered below it appears possible to separate helicity evolution from the unpolarized BK/JIMWLK evolution keeping the approximation and power counting under control, akin to the evolution equation for the QCD Reggeon with saturation corrections derived in [67].

The paper is structured as follows. In Sec. II we define the observables we want to calculate, the quark and anti-quark helicity TMDs and hPDFs. The hPDFs are related to the g_1 structure function and are an essential ingredient in the spin sum rules. We show that these observables depend on the “polarized dipole” operator (16): this is a

¹ Henceforth we will refer to the resummation of powers of $\alpha_s \ln^2 s \sim \alpha_s \ln^2(1/x)$ as the DLA resummation. This is not to be confused with the DLA limit of BFKL evolution, which resums powers of $\alpha_s \ln s \ln Q^2$.

dipole operator in which either the quark or the anti-quark interact with the target in a polarization-dependent way. We construct the main ingredients of the leading-order small- x helicity evolution in Sec. III. The ingredients are the $q \rightarrow qG$, $G \rightarrow q\bar{q}$ and $G \rightarrow GG$ splitting kernels which include helicity dependence. We then study the contributing diagrams in Sec. IV. The main calculation is carried out in Sec. V: there the evolution equations for the fundamental and adjoint polarized dipoles are obtained after one step of small- x helicity evolution and are given in Eqs. (58) and (62) respectively. Just like the equations in Balitsky hierarchy, equations (58) and (62) are not closed, and involve higher-order Wilson-line correlators on their right-hand sides. These are our main general results.

At this point we cross-check our results against those of BER: unfortunately the infrared evolution equations obtained by BER were too complicated to allow for a complete analytic solution, and part of their work including the calculation of the intercept (the power of $1/x$ in the expression for g_1) was done numerically. However, BER had an analytic result for the intercept of their evolution in the case when one neglects the contributions of the non-ladder gluons [1]. Neglecting the non-ladder gluons is not justified by the smallness of any parameter in the problem, and cannot be used as an approximate solution of the problem in the sense of any controlled approximation; nonetheless it is an interesting formal limit where an analytic comparison is possible. In Sec. V we neglect the non-ladder gluon contribution and reproduce the analytic expression for the intercept obtained by BER in the same limit (see Eq. (71)). We thus accomplish a successful cross-check of our technique.

Similar to the case of unpolarized evolution, to obtain a closed equation out of, say, Eq. (58) for the polarized dipole, one has to take the large- N_c limit [68] (with N_c the number of quark colors). Doing so in Sec. VD we obtain a closed system of equations (80) and (82) (along with their linearized version (83)). The solution of these equations (to be found in the future work) would yield the energy dependence of the quark helicity TMD (along with the same energy dependence of the g_1 structure function and $\Delta\Sigma$) in the large- N_c DLA limit.

Quarks are significantly more important for helicity small- x evolution than for the unpolarized BFKL/BK/JIMWLK equations. The quark contribution is neglected in the large- N_c limit of Sec. VD. To preserve the contributions of the quarks we take the large- N_c & N_f limit of Eqs. (58) and (62) in Sec. VE. Here N_f is the number of quark flavors. More precisely, we assume that both N_c and N_f are asymptotically large (in the evolution), while $\alpha_s N_c$ and $\alpha_s N_f$ are fixed and small. In the end we obtain a closed system of equations (87), (88), (89), (90) and (91). Solution of these equations in their linearized form (92), (93) would yield an intercept governing the energy dependence of helicity TMDs, the g_1 structure function and $\Delta\Sigma$ which can be compared with the final (numerical) result of BER. This is left for the future work.

We summarize our results in Sec. VI and discuss potential effects of saturation corrections on small- x helicity evolution.

II. THE OBSERVABLES

To build helicity evolution we need to start by defining which quantity we want to evolve. This is ultimately dictated by the observable we wish to calculate. Let us start with the cross section for semi-inclusive deep inelastic scattering (SIDIS) on a longitudinally polarized target, $\gamma^* + \vec{p} \rightarrow \vec{q} + X$ (with p the target [e.g., proton] and q the produced quark), and the associated quark helicity TMD $g_{1L}(x, k_T)$, both evaluated in small- x kinematics, $s \gg Q^2 \gg k_T^2$. The helicity TMD can be extracted from the SIDIS cross section.

From the analysis of small- x SIDIS and TMDs for polarized targets carried out in [41] we conclude that to calculate $g_{1L}(x, k_T)$ one has to sum up the diagrams shown in Fig. 1 (with all other potentially contributing diagrams canceling out). We assume that the virtual photon is moving along the light-cone “+” direction and work in the $A^+ = 0$ light-cone gauge. As before, the shaded rectangles in Fig. 1 denote the shock wave, though (an example of) the polarization-dependent interaction with the target is shown explicitly on top of the shock wave. If we model our proton as a large nucleus [4–6], which is the standard practice in saturation calculations, we would assume that the polarization-dependent interaction happens with one of the longitudinally polarized nucleons (with a sum over interactions with all polarized nucleons implied). For the real proton one can think of longitudinally polarized partons instead of nucleons, described by some helicity TMD $g_{1L}(x_0, k_T)$ at the initial value x_0 of Bjorken- x . Note that the virtual photon does not interact with the shock wave when it goes through it: diagrams in Fig. 1 are non-zero because we are using light-front perturbation theory (LFPT) [69, 70].

Just like in [41] we begin by writing the quark production cross section in SIDIS, this time based on the diagrams in Fig. 1. The SIDIS cross section is weighted by the polarization of the produced quark σ and is summed over σ as

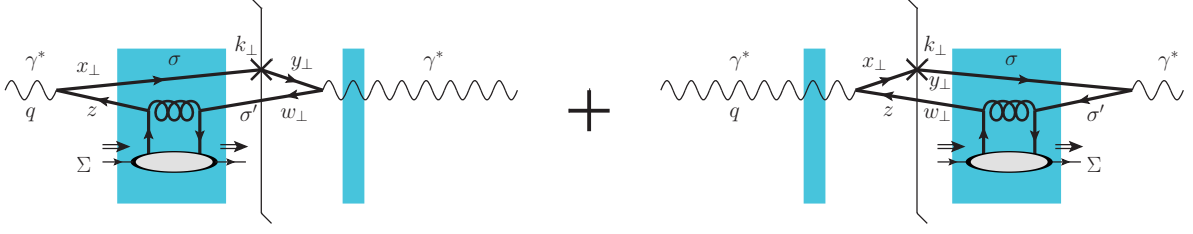


FIG. 1. Diagrams contributing to the quark helicity TMD $g_{1L}^q(x, k_T)$ at small- x .

well to give²

$$\sum_{\sigma} \sigma \frac{d\sigma_{T,L}^{SIDIS}(\sigma)}{d^2k_T} = - \int_{z_i}^1 \frac{dz}{z(1-z)} \int \frac{d^2x_{\perp} d^2y_{\perp} d^2w_{\perp}}{2(2\pi)^3} e^{-ik_{\perp}(\underline{x}-\underline{y})} \sum_{\sigma, \sigma', f} \sigma \Psi_{T,L}^{\gamma^* \rightarrow q\bar{q}}(\underline{x}-\underline{w}, z) \left[\Psi_{T,L}^{\gamma^* \rightarrow q\bar{q}}(\underline{y}-\underline{w}, z) \right]^* \times \left\langle \text{tr} \left[V_{\underline{x}} V_{\underline{w}}^{\dagger}(\sigma') \right] + \text{tr} \left[V_{\underline{w}}(\sigma') V_{\underline{y}}^{\dagger} \right] \right\rangle_{\Sigma}(z), \quad (6)$$

where $\Psi^{\gamma^* \rightarrow q\bar{q}}$ is the light-cone wave function for the $\gamma^* \rightarrow q\bar{q}$ splitting given by

$$\Psi_T^{\gamma^* \rightarrow q\bar{q}}(\underline{x}, z) = \frac{e Z_f}{2\pi} \sqrt{z(1-z)} \left[\delta_{\sigma, -\sigma'} (1-2z-\sigma\lambda) i a_f \frac{\underline{\epsilon}_{\lambda} \cdot \underline{x}}{x_{\perp}} K_1(x_{\perp} a_f) + \delta_{\sigma\sigma'} m_f \sqrt{2} \delta_{\sigma\lambda} K_0(x_{\perp} a_f) \right], \quad (7a)$$

$$\Psi_L^{\gamma^* \rightarrow q\bar{q}}(\underline{x}, z) = \frac{e Z_f}{2\pi} [z(1-z)]^{3/2} 2Q \delta_{\sigma, -\sigma'} K_0(x_{\perp} a_f) \quad (7b)$$

for transverse (T) and longitudinal (L) polarizations of the virtual photon respectively. (Our normalization of light-cone wave functions corresponds to that in [26].) The notation in the above formulas is largely explained in Fig. 1. Here $v^{\pm} \equiv (v^0 \pm v^3)/\sqrt{2}$ for any four-vector $v^{\mu} = (v^+, v^-, \underline{v})$, where \underline{v} is a two-vector in the transverse plane with $v_{\perp} = v_T = |\underline{v}|$. Note that $z = (q^+ - k^+)/k^+$ is the fraction of the virtual photon's (γ^*) light-cone momentum carried by the anti-quark: it is integrated over the range $z_i < z < 1$ with its smallest value $z_i = \Lambda^2/s$, where Λ is the infrared (IR) cutoff and s is the center-of-mass energy squared of the $\gamma^* + p$ system. Above $\sigma, \sigma', \Sigma, \lambda$ are the quark, anti-quark, target, and virtual photon polarizations respectively, and $a_f^2 = z(1-z)Q^2 + m_f^2$ with m_f the mass of quarks of flavor f .

The interaction with the target is described by infinite light-cone Wilson lines in the fundamental representation

$$V_{\underline{x}} = \text{P exp} \left[i g \int_{-\infty}^{\infty} dx^+ A^-(x^+, x^- = 0, \underline{x}) \right]. \quad (8)$$

The trace in Eq. (6) is over matrices in the fundamental representation of $SU(N_c)$. Note that the anti-quark line interaction with the shock wave is denoted by $V_{\underline{w}}^{\dagger}(\sigma')$: this interaction is not completely eikonal, since we need to include a non-eikonal interaction exchanging spin information with the target (the interaction shown explicitly in Fig. 1). Therefore, $V_{\underline{w}}^{\dagger}(\sigma')$ is not entirely a Wilson line of (8), but is a more complicated operator including the spin information in it. The exact formal definition of $V_{\underline{w}}^{\dagger}(\sigma')$ is not important as long as we understand that it stands for an eikonal quark which eventually undergoes a non-eikonal spin-dependent interaction that may turn it into an eikonal gluon. The target averaging of the Wilson line-like operators is denoted by $\langle \dots \rangle_{\Sigma}$: in this case it depends on the target helicity Σ . The argument z of the angle brackets in Eq. (6) labels the longitudinal momentum fraction carried by the polarized line, which in this case is the anti-quark line. (As discussed later, this simple picture is modified by the effects of small- x evolution, such that z can refer to softer partons in the dipole wave function).

Throughout this paper we are interested in extracting the leading- $\ln s$ contributions to the observables we calculate, concentrating on the DLA piece. In the unpolarized evolution case the quark loop depicted in Fig. 1 does not give a

² Let us point out that the analysis in [41] which led to the diagrams in Fig. 1 was performed for the quark TMD (in which the final-state interactions of the produced quark are defined to occur via an unpolarized gauge link), and not for the SIDIS cross section (where they may occur in a polarization-dependent way). Nonetheless, the diagrams in Fig. 1 give us the leading-energy contribution to the SIDIS cross section, which is extracted from Eq. (6) below and is given in Eq. (11). The terms in which the quark line scatters in a polarization-dependent way are not DLA: note that Eq. (6) also contains some non-DLA terms that are neglected in obtaining Eq. (11).

logarithm of energy s . In the polarized SIDIS case at hand it is possible to obtain one logarithm of s from the quark loop. To do so one first has to notice that for $z \ll 1$ and $x_\perp^2 \ll 1/(zQ^2)$ the wave function (7a) simplifies to give (we put $m_f = 0$ for simplicity)

$$\sum_\sigma \sigma \frac{d\sigma_T^{SIDIS}(\sigma)}{d^2k_T} \approx - \int_{z_i}^1 dz \int \frac{d^2x_\perp d^2y_\perp d^2w_\perp}{2(2\pi)^3} e^{-i\mathbf{k}\cdot(\mathbf{x}-\mathbf{y})} \sum_{\sigma',f} (-\sigma') \frac{\alpha_{EM} Z_f^2}{\pi} \frac{\mathbf{x}-\mathbf{w}}{|\mathbf{x}-\mathbf{w}|^2} \cdot \frac{\mathbf{y}-\mathbf{w}}{|\mathbf{y}-\mathbf{w}|^2} \times \left\langle \text{tr} [V_{\mathbf{x}} V_{\mathbf{w}}^\dagger(\sigma')] + \text{tr} [V_{\mathbf{w}}(\sigma') V_{\mathbf{y}}^\dagger] \right\rangle_\Sigma(z) \theta\left(\frac{1}{Q^2} - z|\mathbf{x}-\mathbf{w}|^2\right) \theta\left(\frac{1}{Q^2} - z|\mathbf{y}-\mathbf{w}|^2\right). \quad (9)$$

In arriving at Eq. (9) we concentrated only on transversely-polarized photons, averaging over the polarization λ . We have also dropped the term containing $(\mathbf{x}-\mathbf{w}) \times (\mathbf{y}-\mathbf{w})$, since after integration over x_\perp , y_\perp and w_\perp it should give something proportional to $\underline{k} \times \underline{k} = 0$ because there is no other transverse vector in the problem apart from \underline{k} . The θ -functions in Eq. (9) impose the approximation we have employed ($x_\perp^2 \ll 1/(zQ^2)$ in Eq. (7a)). It is also understood that $z \ll 1$, even though, in the leading-logarithmic spirit we let the z integration range go up to 1.

It is well-known that the leading power of energy in any perturbative QCD interaction is given by the eikonal contribution, which is polarization-independent. Therefore, as we also show explicitly in Appendix A, the polarization-dependent contribution we are after must be energy suppressed. It is convenient to show this dependence explicitly by redefining the averaging in Eqs. (6) and (9) using

$$\langle \dots \rangle_\Sigma(z) = \frac{1}{z s} \langle\langle \dots \rangle\rangle_\Sigma(z), \quad (10)$$

where zs is the center-of-mass energy squared for the anti-quark–proton (or quark–proton) system. (This identity can be understood as the definition of double angle brackets. Note that after the effects of evolution, the factor of $1/(zs)$ always comes in with the momentum fraction z of the polarized line in the dipole.) Employing the substitution (10) in (9) yields

$$\sum_\sigma \sigma \frac{d\sigma_T^{SIDIS}(\sigma)}{d^2k_T} = -\frac{1}{s} \int_{z_i}^1 \frac{dz}{z} \int \frac{d^2x_\perp d^2y_\perp d^2w_\perp}{2(2\pi)^3} e^{-i\mathbf{k}\cdot(\mathbf{x}-\mathbf{y})} \sum_{\sigma',f} (-\sigma') \frac{\alpha_{EM} Z_f^2}{\pi} \frac{\mathbf{x}-\mathbf{w}}{|\mathbf{x}-\mathbf{w}|^2} \cdot \frac{\mathbf{y}-\mathbf{w}}{|\mathbf{y}-\mathbf{w}|^2} \times \left\langle\left\langle \text{tr} [V_{\mathbf{x}} V_{\mathbf{w}}^\dagger(\sigma')] + \text{tr} [V_{\mathbf{w}}(\sigma') V_{\mathbf{y}}^\dagger] \right\rangle\right\rangle_\Sigma(z) \theta\left(\frac{1}{Q^2} - z|\mathbf{x}-\mathbf{w}|^2\right) \theta\left(\frac{1}{Q^2} - z|\mathbf{y}-\mathbf{w}|^2\right). \quad (11)$$

Now we see explicitly that the z -integral is indeed logarithmic: remembering that $z_i = \Lambda^2/s$ we conclude that it gives a logarithm of energy. This is a peculiar feature of helicity-dependent amplitudes: unlike the unpolarized case, quark loops here also generate leading logarithms of energy [1, 60–63, 66].

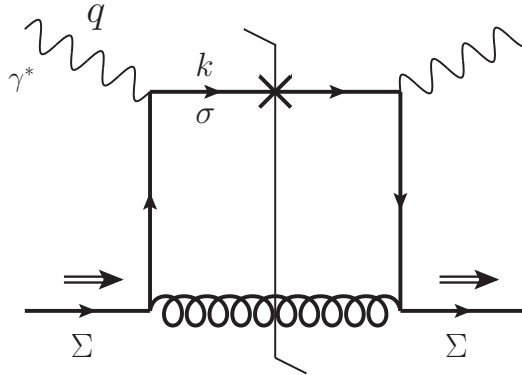


FIG. 2. Lowest-order diagram contributing to the polarized SIDIS cross section on a single quark.

To extract the quark helicity TMD $g_{1L}(x, k_T)$ we consider the lowest-order (LO) SIDIS process on a quark instead of the proton, as pictured in Fig. 2. A simple calculation yields (cf. [41] for the unpolarized quark TMD)

$$\sum_\sigma \sigma \frac{d\sigma_T^{SIDIS}(\sigma)}{d^2k_T} \Big|_{LO} = \frac{4\pi^2 \alpha_{EM}}{s} \sum_f Z_f^2 g_{1L}^{quark}(x, k_T) \Sigma, \quad (12)$$

where Σ is the polarization of the target quark and

$$g_{1L}^{quark}(x, k_T) \Big|_{x \ll 1, m=0} = \frac{\alpha_s C_F}{2\pi^2} \frac{1}{k_T^2} \quad (13)$$

is the small- x lowest-order quark helicity TMD of a target quark as calculated in [71].

Comparing Eqs. (12) and (11) we read off the helicity TMD of a proton (or nuclear) longitudinally polarized target in the leading logarithmic approximation in s :

$$g_{1L}(x, k_T) = -\frac{\Sigma}{4\pi^3} \int_{z_i}^1 \frac{dz}{z} \int \frac{d^2x_\perp d^2y_\perp d^2w_\perp}{2(2\pi)^3} e^{-ik \cdot (x-y)} \frac{\underline{x} - \underline{w}}{|\underline{x} - \underline{w}|^2} \cdot \frac{\underline{y} - \underline{w}}{|\underline{y} - \underline{w}|^2} \\ \times \sum_{\sigma'} (-\sigma') \left\langle \left\langle \text{tr} [V_{\underline{x}} V_{\underline{w}}^\dagger(\sigma')] + \text{tr} [V_{\underline{w}}(\sigma') V_{\underline{y}}^\dagger] \right\rangle \right\rangle_{\Sigma}(z) \theta\left(\frac{1}{Q^2} - z|\underline{x} - \underline{w}|^2\right) \theta\left(\frac{1}{Q^2} - z|\underline{y} - \underline{w}|^2\right). \quad (14)$$

Eq. (14) can be simplified further by noticing that outside the double angle brackets the integrand is invariant under simultaneously replacing $x \leftrightarrow y$ and $\underline{k} \rightarrow -\underline{k}$. At the same time the integral is a function of k_T instead of \underline{k} because there is no other transverse vector in the problem: hence the integral is symmetric under $\underline{k} \rightarrow -\underline{k}$ transformation. Therefore we can simply replace $y \rightarrow x$ in the second trace in the double angle brackets without changing the equality. We get

$$g_{1L}(x, k_T) = -\frac{\Sigma}{4\pi^3} \int_{z_i}^1 \frac{dz}{z} \int \frac{d^2x_\perp d^2y_\perp d^2w_\perp}{2(2\pi)^3} e^{-ik \cdot (x-y)} \frac{\underline{x} - \underline{w}}{|\underline{x} - \underline{w}|^2} \cdot \frac{\underline{y} - \underline{w}}{|\underline{y} - \underline{w}|^2} \\ \times \sum_{\sigma'} (-\sigma') \left\langle \left\langle \text{tr} [V_{\underline{x}} V_{\underline{w}}^\dagger(\sigma')] + \text{tr} [V_{\underline{w}}(\sigma') V_{\underline{x}}^\dagger] \right\rangle \right\rangle_{\Sigma}(z) \theta\left(\frac{1}{Q^2} - z|\underline{x} - \underline{w}|^2\right) \theta\left(\frac{1}{Q^2} - z|\underline{y} - \underline{w}|^2\right). \quad (15)$$

So far we have only calculated the energy dependence coming from a single quark loop. The energy dependence of the longitudinally polarized SIDIS cross section (6) and the quark helicity TMD (15) mainly comes from the correlator of Wilson lines. We conclude that to find either of these quantities in the small- x regime we need to evolve the *polarized dipole* operator

$$\left\langle \left\langle \text{tr} [V_{\underline{x}} V_{\underline{y}}^\dagger(\sigma)] + \text{tr} [V_{\underline{y}}(\sigma) V_{\underline{x}}^\dagger] \right\rangle \right\rangle_{\Sigma}(z) \quad (16)$$

in z (the momentum fraction of the polarized line).

Other observables would benefit from constructing the small- x evolution of the polarized dipole. Knowing the helicity TMD (15) would allow one to construct the quark hPDF,

$$\Delta q(x, Q^2) = \int d^2k_T g_{1L}(x, k_T) = -\frac{\Sigma}{4\pi^3} \int_{z_i}^1 \frac{dz}{z} \int \frac{d^2x_\perp d^2w_\perp}{4\pi} \frac{1}{|\underline{x} - \underline{w}|^2} \theta\left(\frac{1}{Q^2} - z|\underline{x} - \underline{w}|^2\right) \\ \times \sum_{\sigma'} (-\sigma') \left\langle \left\langle \text{tr} [V_{\underline{x}} V_{\underline{w}}^\dagger(\sigma')] + \text{tr} [V_{\underline{w}}(\sigma') V_{\underline{x}}^\dagger] \right\rangle \right\rangle_{\Sigma}(z). \quad (17)$$

The integrals over x_\perp and w_\perp in Eq. (17) now have a singularity at $\underline{x} = \underline{w}$: it is regulated by requiring that $|\underline{x} - \underline{w}| > \rho$, where $\rho^2 = 1/(zs)$ is the shortest allowed distance (squared) in the problem. We note in passing that the transverse space integrals in Eq. (17) now bring in another logarithm of energy, in part due to the ultra-violet (UV) cutoff ρ , and in part due to the z -dependent IR cutoff resulting from the θ -function. Combining this with the energy logarithm coming from the z integration, we observe that the quark loop in Fig. 1 leads to two logarithms of energy. This is our first example of how the DLA appears in a calculation.

Knowing $\Delta q(x, Q^2)$ one can calculate the (leading-twist) structure function $g_1(x, Q^2)$ from Eq. (5) above along with $\Delta\Sigma$ and its contribution to S_q in the spin sum rule (1). Note that Eqs. (6), (12) and (5) allow one to write down an

all-twist expression for $g_1(x, Q^2)$, without extracting the leading-energy (DLA) contribution from the quark loop:

$$\begin{aligned}
g_1(x, Q^2) &= \frac{s \Sigma}{2\pi^2 \alpha_{EM}} \int d^2 k_\perp \sum_\sigma \sigma \left[\frac{d\sigma_T^{SIDIS}(\sigma)}{d^2 k_T} + \frac{d\sigma_L^{SIDIS}(\sigma)}{d^2 k_T} \right] \\
&= -\frac{\Sigma}{2\pi^2 \alpha_{EM}} \int_{z_i}^1 \frac{dz}{z^2(1-z)} \int \frac{d^2 x_\perp d^2 w_\perp}{4\pi} \sum_{\sigma, \sigma', f} \sigma \left[\frac{1}{2} \sum_\lambda \left| \Psi_T^{\gamma^* \rightarrow q\bar{q}}(\underline{x} - \underline{w}, z) \right|^2 + \left| \Psi_L^{\gamma^* \rightarrow q\bar{q}}(\underline{x} - \underline{w}, z) \right|^2 \right] \\
&\times \left\langle \left\langle \text{tr} \left[V_{\underline{x}} V_{\underline{w}}^\dagger(\sigma') \right] + \text{tr} \left[V_{\underline{w}}(\sigma') V_{\underline{x}}^\dagger \right] \right\rangle \right\rangle_\Sigma(z). \tag{18}
\end{aligned}$$

We see that the x -dependence of $g_1(x, Q^2)$ (either from Eq. (5) or its more precise version in Eq. (18)) and $\Delta\Sigma(x, Q^2)$ is also determined by the energy dependence of the correlator (16). Hence the small- x evolution of the operator (16) would allow us to address many important observables, including the ones relevant for the spin puzzle.

III. THE INGREDIENTS

We want to derive s -channel helicity evolution equations, similar to the BK/JIMWLK equations [13–20], but now for the polarization-dependent dipole operator in Eq. (16). Following the standard technique we will continue working in the light-cone gauge of the dipole, that is, as our projectile is moving along the light-cone x^+ direction, we will employ the $A^+ = 0$ light-cone gauge.

Before we can even start discussing the diagrams relevant for the helicity evolution, we observe that small- x evolution in the $A^+ = 0$ gauge takes place in the light-cone wave function [69, 70] of the dipole projectile. Hence, to write down s -channel helicity evolution equations we will need the basic helicity-dependent light-cone wave functions describing the $q \rightarrow qG$, $G \rightarrow q\bar{q}$ and $G \rightarrow GG$ transitions, which are the building blocks of any evolution equation. They can be obtained from [26], or they can be derived independently. For simplicity we assume that all the quarks are massless, $m = 0$, since, as one can show using the analysis below, mass corrections do not contribute to the double-logarithmic (DLA) small- x evolution.

A. $q \rightarrow qG$ Splitting

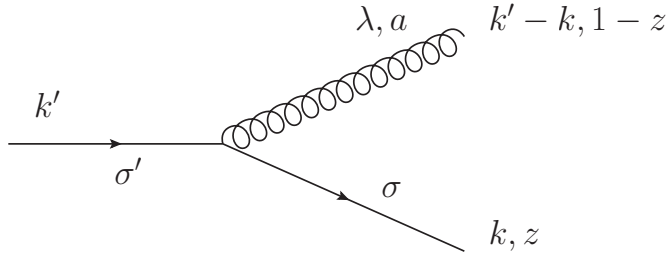


FIG. 3. Leading-order diagram contributing to the light-cone wave function for $q \rightarrow qG$.

Consider the $q \rightarrow qG$ splitting depicted in Fig. 3. The exact leading-order in α_s momentum-space light-cone wave function is

$$\psi^{q \rightarrow qG} = -g t^a \delta_{\sigma\sigma'} \sqrt{z} \frac{\epsilon_\lambda^* \cdot (\underline{k} - z\underline{k}')}{|\underline{k} - z\underline{k}'|^2} [1 + z + \sigma \lambda (1 - z)]. \tag{19}$$

Here $0 \leq z \leq 1$, where $z = k^+/k'^+$, σ and σ' are the quark polarizations, λ and a are the gluon polarization and color, and t^a are the fundamental $SU(N_c)$ generators. All the labels are explained in Fig. 3. We are using light-front perturbation theory (LFPT) rules [69, 70] with all the quark and gluon polarizations quantized along the same z -axis (beam axis) direction. The gluon polarization four-vector in the $A^+ = 0$ light-cone gauge is

$$\epsilon_\lambda^\mu(k) = \left(0, \frac{\epsilon_\lambda \cdot \underline{k}}{k^+}, \epsilon_\lambda \right). \tag{20}$$

Since we are interested in small- x evolution, we will only need the cases when either the outgoing quark or the gluon are very soft, i.e., carry a small fraction of the “+” momentum of the incoming quark. The relevant limits are

$$\psi^{q \rightarrow qG} \Big|_{z \rightarrow 0} \approx -g t^a \delta_{\sigma\sigma'} \sqrt{z} \frac{\epsilon_\lambda^* \cdot \underline{k}}{|\underline{k}|^2} [1 + \sigma \lambda] \quad (21)$$

(soft outgoing quark) and

$$\psi^{q \rightarrow qG} \Big|_{z \rightarrow 1} \approx g t^a \delta_{\sigma\sigma'} \frac{\epsilon_\lambda^* \cdot (\underline{k}' - \underline{k})}{|\underline{k}' - \underline{k}|^2} [2 + \sigma \lambda (1 - z) + \dots] \quad (22)$$

(soft gluon). In the latter we keep only the spin-dependent part of the sub-eikonal corrections.

Fourier-transforming Eqs. (21) and (22) into transverse coordinate space we get

$$\psi^{q \rightarrow qG} \Big|_{z \rightarrow 0} \approx -\frac{i g t^a}{2\pi} \delta_{\sigma\sigma'} \sqrt{z} \frac{\epsilon_\lambda^* \cdot \underline{x}}{|\underline{x}|^2} [1 + \sigma \lambda] \quad (23)$$

and

$$\psi^{q \rightarrow qG} \Big|_{z \rightarrow 1} \approx \frac{i g t^a}{2\pi} \delta_{\sigma\sigma'} \frac{\epsilon_\lambda^* \cdot \underline{x}}{|\underline{x}|^2} [2 + \sigma \lambda (1 - z) + \dots], \quad (24)$$

where \underline{x} is the transverse vector separating the soft quark from the position of the incoming quark in Eq. (23), while in Eq. (24) it denotes the transverse separation between the soft gluon and the incoming quark. Note that Eqs. (19), (21), (22), (23) and (24) are also valid for the anti-quark splitting, $\bar{q} \rightarrow \bar{q}G$.

B. $G \rightarrow q\bar{q}$ Splitting

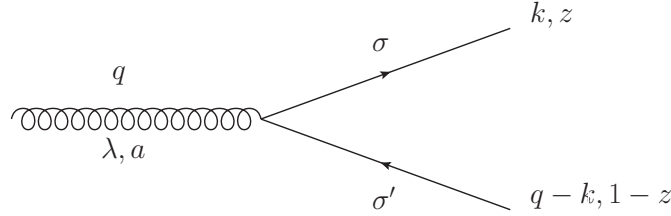


FIG. 4. Leading-order diagram contributing to the light-cone wave function for $G \rightarrow q\bar{q}$.

Now we consider the $G \rightarrow q\bar{q}$ splitting. The exact leading- α_s light-cone wave function is

$$\psi^{G \rightarrow q\bar{q}} = g t^a \sqrt{z(1-z)} \frac{\epsilon_\lambda \cdot (\underline{k} - z\underline{q})}{|\underline{k} - z\underline{q}|^2} \delta_{\sigma, -\sigma'} [1 - 2z - \sigma \lambda]. \quad (25)$$

The soft-quark limit is

$$\psi^{G \rightarrow q\bar{q}} \Big|_{z \rightarrow 0} \approx g t^a \sqrt{z} \frac{\epsilon_\lambda \cdot \underline{k}}{|\underline{k}|^2} \delta_{\sigma, -\sigma'} [1 - \sigma \lambda], \quad (26)$$

and the soft-antiquark limit is

$$\psi^{G \rightarrow q\bar{q}} \Big|_{z \rightarrow 1} \approx g t^a \sqrt{1-z} \frac{\epsilon_\lambda \cdot (\underline{q} - \underline{k})}{|\underline{q} - \underline{k}|^2} \delta_{\sigma, -\sigma'} [1 - \sigma' \lambda]. \quad (27)$$

Here again we only keep the polarization-dependent sub-eikonal corrections. Fourier-transforming into transverse coordinate space gives

$$\psi^{G \rightarrow q\bar{q}} \Big|_{z \rightarrow 0} \approx \frac{i g t^a}{2\pi} \sqrt{z} \frac{\epsilon_\lambda \cdot \underline{x}}{|\underline{x}|^2} \delta_{\sigma, -\sigma'} [1 - \sigma \lambda] \quad (28)$$

and

$$\psi^{G \rightarrow q\bar{q}} \Big|_{z \rightarrow 1} \approx \frac{i g t^a}{2\pi} \sqrt{1-z} \frac{\epsilon_\lambda \cdot \underline{x}}{|\underline{x}|^2} \delta_{\sigma, -\sigma'} [1 - \sigma' \lambda], \quad (29)$$

where \underline{x} is again the transverse vector connecting the position of the incoming gluon with that of a soft (anti-)quark.

C. $G \rightarrow GG$ Splitting

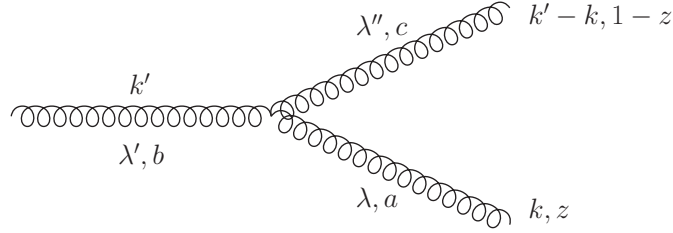


FIG. 5. Leading-order diagram contributing to the light-cone wave function for $G \rightarrow GG$.

Finally, let us consider the $G \rightarrow GG$ splitting. The exact leading-order light-cone wave function is

$$\psi^{G \rightarrow GG} = 2 i g f^{abc} \frac{z(1-z)}{|\underline{k} - z\underline{k}'|^2} \left[\frac{1}{1-z} \underline{\epsilon}_{\lambda''}^* \cdot (\underline{k} - z\underline{k}') \underline{\epsilon}_{\lambda}^* \cdot \underline{\epsilon}_{\lambda'} + \frac{1}{z} \underline{\epsilon}_{\lambda}^* \cdot (\underline{k} - z\underline{k}') \underline{\epsilon}_{\lambda''}^* \cdot \underline{\epsilon}_{\lambda'} - \underline{\epsilon}_{\lambda'} \cdot (\underline{k} - z\underline{k}') \underline{\epsilon}_{\lambda''}^* \cdot \underline{\epsilon}_{\lambda}^* \right]. \quad (30)$$

The soft-gluon limit is

$$\begin{aligned} \psi^{G \rightarrow GG} \Big|_{z \rightarrow 0} &\approx 2 i g f^{abc} \frac{z}{\underline{k}^2} \left[\frac{1}{z} \underline{\epsilon}_{\lambda}^* \cdot \underline{k} \underline{\epsilon}_{\lambda''}^* \cdot \underline{\epsilon}_{\lambda'} - \underline{\epsilon}_{\lambda}^* \cdot \underline{k}' \underline{\epsilon}_{\lambda''}^* \cdot \underline{\epsilon}_{\lambda'} \right. \\ &\quad \left. + \underline{\epsilon}_{\lambda''}^* \cdot \underline{k} \underline{\epsilon}_{\lambda}^* \cdot \underline{\epsilon}_{\lambda'} - \underline{\epsilon}_{\lambda'} \cdot \underline{k} \underline{\epsilon}_{\lambda''}^* \cdot \underline{\epsilon}_{\lambda}^* + \dots \right] \\ &= 2 i g f^{abc} \frac{z}{\underline{k}^2} \left[\frac{1}{z} \underline{\epsilon}_{\lambda}^* \cdot \underline{k} \delta_{\lambda''\lambda'} - \underline{\epsilon}_{\lambda}^* \cdot \underline{k}' \delta_{\lambda''\lambda'} \right. \\ &\quad \left. + \underline{\epsilon}_{\lambda''}^* \cdot \underline{k} \delta_{\lambda\lambda'} + \underline{\epsilon}_{\lambda'} \cdot \underline{k} \delta_{\lambda'',-\lambda} + \dots \right], \end{aligned} \quad (31)$$

where again we only keep the sub-eikonal terms which transfer polarization information to the softer gluon. Fourier-transforming into transverse coordinate space gives

$$\psi^{G \rightarrow GG} \Big|_{z \rightarrow 0} \approx \frac{-g f^{abc}}{\pi} \frac{z}{\underline{x}^2} \left[\frac{1}{z} \underline{\epsilon}_{\lambda}^* \cdot \underline{x} \delta_{\lambda''\lambda'} + \underline{\epsilon}_{\lambda''}^* \cdot \underline{x} \delta_{\lambda\lambda'} + \underline{\epsilon}_{\lambda'} \cdot \underline{x} \delta_{\lambda'',-\lambda} + \dots \right], \quad (32)$$

where the transverse vector \underline{x} connects the position of the incoming gluon with that of the soft gluon.

D. Evolution Kernels

For future purposes it is instructive to square the wave functions obtained above in order to understand the mechanism for generating the double logarithms that we want to resum and to obtain evolution kernels for the ladder part of the evolution. Squaring the coordinate-space wave functions of Sections III A, B and C we can construct the splitting kernels illustrated in Fig. 6 in a matrix form, by analogy to BER [1]. The shaded rectangles denote the shock wave, which encodes both the subsequent evolution and the interaction with the longitudinally polarized target. We assume that the amplitude these wave functions squared connect to at the bottom is forward in color and flavor (and of course in transverse positions); for a longitudinally-polarized target, it is also automatically forward in helicity. This assumption can be explicitly checked by the lowest-order diagram calculations (akin to that done above for the graph in Fig. 2), which provide the initial conditions for our evolution (see Appendix A). Since those amplitudes are independent of color and flavor, we sum over the colors of soft quarks and gluons, and also over flavors of the quarks in the lower left panel of Fig. 6. We also sum over polarizations and colors of the hard quarks and gluons going through the shock wave, since in the DLA the interactions of those particles with the shock wave can be neglected. (Those interactions are at most single-logarithmic.)

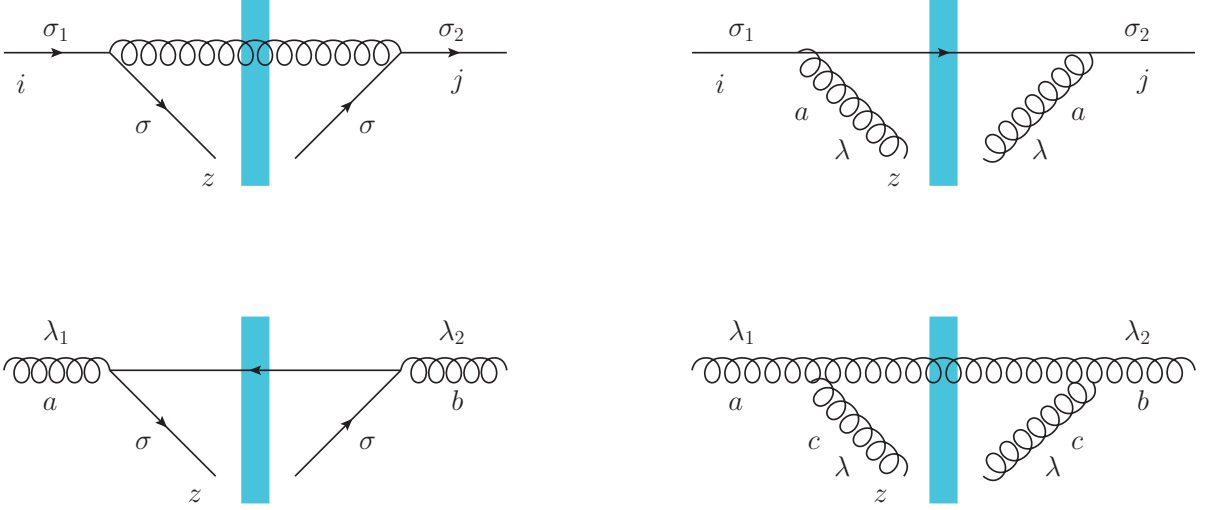


FIG. 6. Splitting kernels for the ladder part of helicity evolution.

The resulting kernels are (going left to right in each row of Fig. 6 and keeping only the polarization-dependent sub-eikonal part of the splitting kernel)

$$K^{q\bar{q} \rightarrow q\bar{q}} = \frac{\alpha_s C_F}{2\pi^2} \delta_{\sigma_1\sigma} \delta_{\sigma_2\sigma} \delta_{ij} \int dz \int \frac{d^2 x_\perp}{x_\perp^2}, \quad (33a)$$

$$K^{q\bar{q} \rightarrow GG} = \frac{\alpha_s C_F}{2\pi^2} \delta_{\sigma_1\sigma_2} \sigma_1 \lambda \delta_{ij} \int dz \int \frac{d^2 x_\perp}{x_\perp^2}, \quad (33b)$$

$$K^{GG \rightarrow q\bar{q}} = \frac{\alpha_s N_f}{4\pi^2} \delta_{\lambda_1\lambda_2} \delta_{\sigma,-\lambda_1} \delta^{ab} \int dz \int \frac{d^2 x_\perp}{x_\perp^2}, \quad (33c)$$

$$K^{GG \rightarrow GG} = \frac{\alpha_s N_c}{\pi^2} \delta_{\lambda_1\lambda_2} \lambda \lambda_1 \delta^{ab} \int dz \int \frac{d^2 x_\perp}{x_\perp^2}. \quad (33d)$$

At first glance the kernels in Eq. (33) appear completely irrelevant to the task at hand: the integrals over longitudinal momentum fractions z in those kernels are not logarithmic. Moreover, the only integral in the kernels of Eq. (33) that may generate a logarithm is the integral over x_\perp . However, in the unpolarized BFKL evolution [10–20] (in coordinate space) such integrals are usually cut off by some transverse momentum scale, e.g., by Q^2 in DIS, and do not become logarithms of energy. Hence our usual unpolarized small- x (gluon) evolution intuition appears to tell us that the emission kernels in Fig. 6 and Eq. (33) cannot generate the DLA powers of $\alpha_s \ln^2 s \sim \alpha_s \ln^2(1/x)$.

Indeed the above concerns, while legitimate, are incorrect. An example of the DLA evolution in the s -channel transverse coordinate space formalism at hand is given in [67] for the case of the QCD Reggeon. Just like in [67] we show in Appendix A that the initial conditions for the helicity-dependent evolution are given by an energy suppressed cross-section $\hat{\sigma} \sim 1/(zs)$, where s is the center-of-mass energy squared of the system and z is the longitudinal momentum fraction of the softest parton in the cascade. Hence all the kernels in Eq. (33) would act on $1/z$ in the initial condition or in the subsequent evolution. This would make the z -integrals logarithmic, $\int dz/z$, yielding us one power of $\ln s$ per each splitting. The other $\ln s$ arises from the x_\perp -integral in Eq. (33). As will become apparent later, and by analogy to what was already observed after Eq. (17) and in [67], in the case of our helicity evolution the x_\perp -integrals will be divergent in the ultra-violet (UV) and will be regulated by the inverse center-of-mass energy of the system. In addition, the infra-red (IR) cutoff on the x_\perp -integral will be z -dependent, and would also generate a logarithm of energy. We see that each integral in Eq. (33) contributes a logarithm of s , yielding $\alpha_s \ln^2 s$ per each splitting, and hence contributing to the DLA approximation we are constructing.

IV. DLA DIAGRAMS: LADDERS AND NON-LADDERS

Our goal is to construct the small- x evolution of the polarized dipole operator in Eq. (16). In this Section we will explore the contributing diagrams using the evolution building blocks developed in Sec. III. The most natural guess for the types of diagrams one has to resum to obtain DLA helicity evolution would be quark and gluon ladders shown

in Fig. 7. In [67] it was the quark ladder (i.e., a ladder with quarks in the t -channel and with gluon rungs) that gave the small- x evolution of the QCD Reggeon.

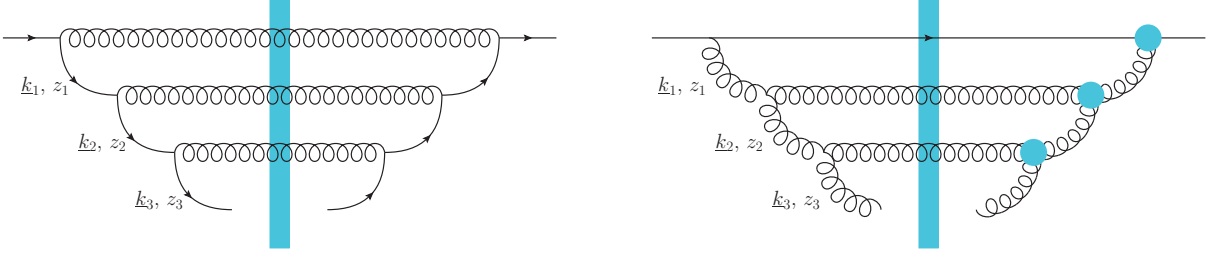


FIG. 7. Examples of the quark and gluon ladder diagrams. Non-eikonal gluon emission vertices are denoted by shaded circles.

Let us first discuss how the ladders give double logarithms. We begin with the quark ladder, depicted also in the left panel of Fig. 7. The longitudinal momentum fractions carried by the quarks (and the gluons going through the shock wave) are ordered, $1 \gg z_1 \gg z_2 \gg z_3 \gg \dots$. As one can see from Eq. (21) (and, in a general case, also from Eq. (26)), each emission of a soft quark generates a factor of \sqrt{z} . The quark ladder in Fig. 7 then yields

$$\int_{z_i}^1 \frac{dz_1}{z_1} \int_{z_i}^{z_1} \frac{dz_2}{z_2} \int_{z_i}^{z_2} \frac{dz_3}{z_3} (\sqrt{z_1})^2 \left(\sqrt{\frac{z_2}{z_1}}\right)^2 \left(\sqrt{\frac{z_3}{z_2}}\right)^2 = \int_{z_i}^1 \frac{dz_1}{z_1} \int_{z_i}^{z_1} \frac{dz_2}{z_2} \int_{z_i}^{z_2} \frac{dz_3}{z_3} z_3. \quad (34)$$

The factor of z_3 here is canceled by the energy-suppressed initial conditions, which, just like in Eq. (10) (or in Eq. (12)) bring in a factor of $1/(z_3 s)$. We thus get a logarithmic contribution from the integral in Eq. (34). Hence one condition for the DLA contribution is the longitudinal momentum ordering,

$$1 \gg z_1 \gg z_2 \gg z_3 \gg \dots \quad (35)$$

Gluon ladders also give a contribution similar to Eq. (34). Consider the ladder in the right panel of Fig. 7. To transfer polarization information down the ladder, one of the quark-gluon vertices (either to the left or right of the shock wave) has to be sub-eikonal: according to Eq. (22), this means that the eikonal vertex brings in a factor of 1 (in term of counting the powers of z_1), while the sub-eikonal vertex gives a power of z_1 . We denote sub-eikonal gluon emission vertices by the shaded circle in Fig. 7: note that the circle could be on either side of the shock wave, and the diagram on the right of Fig. 7 represents only one realization of the gluon ladder. The situation repeats itself for the triple gluon vertices, as follows from Eq. (31): in the emission of an s -channel gluon, one of the vertices (either to the left or right of the shock wave, denoted by the shaded circle too) has to be sub-eikonal. (We neglect the contribution of both vertices being sub-eikonal, since this is even more energy-suppressed than helicity evolution and is beyond our DLA here.) For the gluon ladder on the right of Fig. 7 we get

$$\int_{z_i}^1 \frac{dz_1}{z_1} \int_{z_i}^{z_1} \frac{dz_2}{z_2} \int_{z_i}^{z_2} \frac{dz_3}{z_3} z_1 \frac{z_2}{z_1} \frac{z_3}{z_2} = \int_{z_i}^1 \frac{dz_1}{z_1} \int_{z_i}^{z_1} \frac{dz_2}{z_2} \int_{z_i}^{z_2} \frac{dz_3}{z_3} z_3, \quad (36)$$

which again is a logarithmic contribution.

To obtain a DLA contribution we also need to get energy logarithms coming from the integrals over transverse momenta. This is achievable only if the softest gluon dominates in the energy denominator, just like in small- x evolution. After a little bit of work one can show that this translates into the following condition (cf. Eq. (2.31) in [1])

$$\frac{k_1^2}{z_1} \ll \frac{k_2^2}{z_2} \ll \frac{k_3^2}{z_3} \ll \dots \quad (37)$$

In transverse coordinate space this condition becomes

$$z_1 \underline{x}_1^2 \gg z_2 \underline{x}_2^2 \gg z_3 \underline{x}_3^2 \gg \dots, \quad (38)$$

where the vectors \underline{x}_n are Fourier conjugates of \underline{k}_n . The ordering (38) leads to transverse coordinate integrals like

$$\int \frac{x_{n-1,\perp}^2 z_{n-1}/z_n}{1/(z_n s)} \frac{dx_{n,\perp}^2}{x_{n,\perp}^2}, \quad (39)$$

where the UV divergence gets regulated by the inverse of the largest momentum scale squared associated with the emission of the n th parton, $1/(z_n s)$. As discussed above (see discussions below Eq. (17) and at the end of Sec. IIID), the transverse integrals like (39) in helicity evolution generate logarithms of energy coming both from their UV and IR cutoffs.

We conclude that for ladder diagrams like those in Fig. 7, emission of each s -channel gluon generates a power of α_s along with two logarithms of energy: one logarithm comes from the integration over longitudinal momentum fractions, like that in (34), while another logarithm of energy comes from the transverse coordinate (or momentum) integrals (39). This latter feature is the essential difference between the helicity evolution and the unpolarized evolution: in the latter the transverse integrals do not generate logarithms of energy and resummation is single-logarithmic.

Let us point out that in helicity evolution quark and gluon ladders of Fig. 7 can mix, as follows from Fig. 6 [1]. This is in analogy to the Q^2 evolution of the Dokshitzer–Gribov–Lipatov–Altarelli–Parisi (DGLAP) equation [72–74].

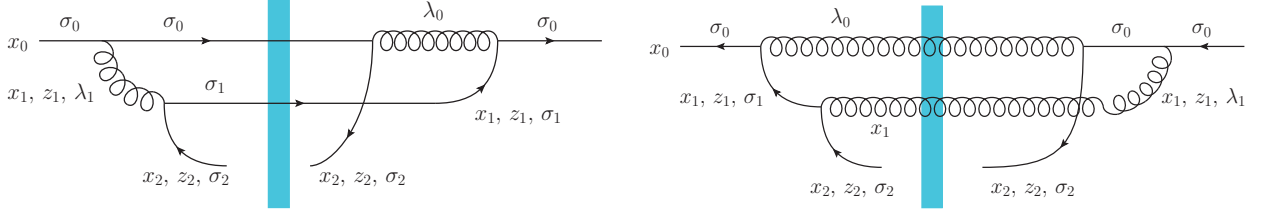


FIG. 8. Examples of non-ladder diagrams involving quarks.

However DLA evolution is not limited to ladder diagrams. There exist non-ladder diagrams which also yield a DLA contribution. We will refer to diagrams as “non-ladder” if they contain an s -channel parton with longitudinal momentum fraction z_n which was not emitted by the parton with the longitudinal momentum fraction z_{n-1} , but instead was emitted by the parton with the fraction z_m with $m < n - 1$. (The ordering (35) is implied in this definition.) Examples of diagrams involving a non-ladder quark emission are shown in Fig. 8. The diagram in the left panel depicts helicity evolution of a polarized quark Wilson line, while the diagram in the right panel depicts helicity evolution of a polarized anti-quark Wilson line. Both graphs lead to a polarized anti-quark Wilson line at the bottom of the evolution.

To analyze the diagrams in Fig. 8 we first of all notice that requiring that $1 \gg z_1 \gg z_2$ works on both sides of the shock wave giving a “logarithmic” contribution

$$\sim \int_{z_i}^1 \frac{dz_1}{z_1} \int_{z_i}^{z_1} \frac{dz_2}{z_2} z_2 \quad (40)$$

only if we assume that the vertex emitting gluon z_1 is eikonal in both graphs of Fig. 8. The transverse position integrals are more complicated. Noting that all other vertices are non-eikonal and polarization-dependent, the transverse coordinate and polarization dependence of the diagram in the left panel of Fig. 8 becomes (the factor of σ_2 comes from the initial condition, or, equivalently, from the interaction with the target)

$$\begin{aligned} & - \sum_{\lambda_0, \lambda_1, \sigma_1, \sigma_2} \int d^2 x_1 d^2 x_2 \frac{\epsilon_{\lambda_1} \cdot \underline{x}_{21}}{x_{21}^2} \frac{\epsilon_{\lambda_1}^* \cdot \underline{x}_{10}}{x_{10}^2} \frac{\epsilon_{\lambda_0} \cdot \underline{x}_{10}}{x_{10}^2} \frac{\epsilon_{\lambda_0}^* \cdot \underline{x}_{20}}{x_{20}^2} \delta_{\sigma_1, -\sigma_2} (1 - \sigma_2 \lambda_1) \delta_{\sigma_0 \sigma_1} (1 + \sigma_0 \lambda_0) \delta_{\sigma_0, -\sigma_2} (1 - \sigma_2 \lambda_0) \sigma_2 \\ & = - \sum_{\lambda_0, \lambda_1, \sigma_2} \int d^2 x_1 d^2 x_2 \frac{\epsilon_{\lambda_1} \cdot \underline{x}_{21}}{x_{21}^2} \frac{\epsilon_{\lambda_1}^* \cdot \underline{x}_{10}}{x_{10}^2} \frac{\epsilon_{\lambda_0} \cdot \underline{x}_{10}}{x_{10}^2} \frac{\epsilon_{\lambda_0}^* \cdot \underline{x}_{20}}{x_{20}^2} \delta_{\sigma_0, -\sigma_2} (1 - \sigma_2 \lambda_1) (1 + \sigma_0 \lambda_0) (1 - \sigma_2 \lambda_0) \sigma_2 \\ & = 4 \sigma_0 \sum_{\lambda_0, \lambda_1} \int d^2 x_1 d^2 x_2 \frac{\epsilon_{\lambda_1} \cdot \underline{x}_{21}}{x_{21}^2} \frac{\epsilon_{\lambda_1}^* \cdot \underline{x}_{10}}{x_{10}^2} \frac{\epsilon_{\lambda_0} \cdot \underline{x}_{10}}{x_{10}^2} \frac{\epsilon_{\lambda_0}^* \cdot \underline{x}_{20}}{x_{20}^2} \delta_{\lambda_0 \lambda_1} (1 + \lambda_1 \sigma_0) \\ & = 2 \int d^2 x_1 d^2 x_2 \frac{1}{x_{10}^2 x_{21}^2 x_{20}^2} [\sigma_0 \underline{x}_{21} \cdot \underline{x}_{20} - i \underline{x}_{21} \times \underline{x}_{20}], \end{aligned} \quad (41)$$

where the cross-product of two transverse vectors is defined as $\underline{u} \times \underline{v} = u_x v_y - u_y v_x$, while $\underline{x}_{ij} = \underline{x}_i - \underline{x}_j$ and $x_{ij} = |\underline{x}_{ij}|$. In arriving at Eq. (41) we have used the ingredients worked out in Sec. III. We note that the x_2 -integral in the σ_0 -dependent term is logarithmic only in the IR when $x_{21} \sim x_{20} \gg x_{10}$. The term with the cross product in Eq. (41) is independent of polarization and could be neglected.

However there is no need to do that, because the whole contribution of the diagram in the left panel of Fig. 8 is canceled by the diagram in the right panel of the same figure. Indeed a similar calculation keeping only the transverse

coordinate and polarization dependence of the diagram in the right panel of Fig. 8 yields

$$\begin{aligned}
& - \sum_{\lambda_0, \lambda_1, \sigma_1, \sigma_2} \int d^2 x_1 d^2 x_2 \frac{\underline{\epsilon}_{\lambda_0}^* \cdot \underline{x}_{10}}{x_{10}^2} \frac{\underline{\epsilon}_{\lambda_1}^* \cdot \underline{x}_{21}}{x_{21}^2} \frac{\underline{\epsilon}_{\lambda_0} \cdot \underline{x}_{20}}{x_{20}^2} \frac{\underline{\epsilon}_{\lambda_1} \cdot \underline{x}_{10}}{x_{10}^2} \delta_{\sigma_0 \sigma_1} (1 + \sigma_0 \lambda_0) \delta_{\sigma_1 \sigma_2} (1 + \sigma_1 \lambda_1) \delta_{\sigma_0 \sigma_2} (1 + \sigma_0 \lambda_0) \sigma_2 \\
& = - \sum_{\lambda_0, \lambda_1, \sigma_2} \int d^2 x_1 d^2 x_2 \frac{\underline{\epsilon}_{\lambda_0}^* \cdot \underline{x}_{10}}{x_{10}^2} \frac{\underline{\epsilon}_{\lambda_1}^* \cdot \underline{x}_{21}}{x_{21}^2} \frac{\underline{\epsilon}_{\lambda_0} \cdot \underline{x}_{20}}{x_{20}^2} \frac{\underline{\epsilon}_{\lambda_1} \cdot \underline{x}_{10}}{x_{10}^2} \delta_{\sigma_0 \sigma_2} (1 + \sigma_0 \lambda_0)^2 (1 + \sigma_2 \lambda_1) \sigma_2 \\
& = - \sum_{\lambda_0, \lambda_1} \int d^2 x_1 d^2 x_2 \frac{\underline{\epsilon}_{\lambda_0}^* \cdot \underline{x}_{10}}{x_{10}^2} \frac{\underline{\epsilon}_{\lambda_1}^* \cdot \underline{x}_{21}}{x_{21}^2} \frac{\underline{\epsilon}_{\lambda_0} \cdot \underline{x}_{20}}{x_{20}^2} \frac{\underline{\epsilon}_{\lambda_1} \cdot \underline{x}_{10}}{x_{10}^2} 2 (1 + \sigma_0 \lambda_0) (1 + \sigma_0 \lambda_1) \sigma_0 \\
& = - \sum_{\lambda_0, \lambda_1} \int d^2 x_1 d^2 x_2 \frac{\underline{\epsilon}_{\lambda_0}^* \cdot \underline{x}_{10}}{x_{10}^2} \frac{\underline{\epsilon}_{\lambda_1}^* \cdot \underline{x}_{21}}{x_{21}^2} \frac{\underline{\epsilon}_{\lambda_0} \cdot \underline{x}_{20}}{x_{20}^2} \frac{\underline{\epsilon}_{\lambda_1} \cdot \underline{x}_{10}}{x_{10}^2} 2 [(1 + \lambda_0 \lambda_1) \sigma_0 + \lambda_0 + \lambda_1] \\
& = -2 \int \frac{d^2 x_1 d^2 x_2}{x_{10}^2 x_{21}^2 x_{20}^2} [\sigma_0 \underline{x}_{21} \cdot \underline{x}_{20} - i \underline{x}_{10} \times \underline{x}_{21}]. \tag{42}
\end{aligned}$$

The remaining factors in both diagrams in Fig. 8, such as the color factors and z -integrals are identical in the DLA. Hence the diagrams in the two panels of Fig. 8 cancel each other when added together, as can be seen by comparing Eqs. (41) and (42). One may rightfully worry that the left panel of Fig. 8 gives a contribution to the DLA evolution of a quark, while the right panel contributes to the anti-quark evolution. However, our polarized dipole operator (16) contains a sum of the polarized quark and anti-quark line contributions taken at the same transverse coordinates. (The remaining anti-quark and quark lines are unpolarized and cannot be involved in non-ladder quark emission/absorption.) We conclude that the non-ladder quark diagrams in Fig. 8 do not contribute to the DLA evolution of the polarized dipole operator (16).

The argument can be generalized to include all non-ladder quark emissions. For this one can imagine “dressing” the diagrams from Fig. 8 with higher-order DLA ladder corrections. One can then argue that such corrections would not affect the cancellation. For a complete analysis one has to include the left-right mirror images of the diagrams in Fig. 8 and allow for non-ladder gluons too. Hence non-ladder quarks in general do not contribute to the DLA evolution of the polarized dipole operator (16).

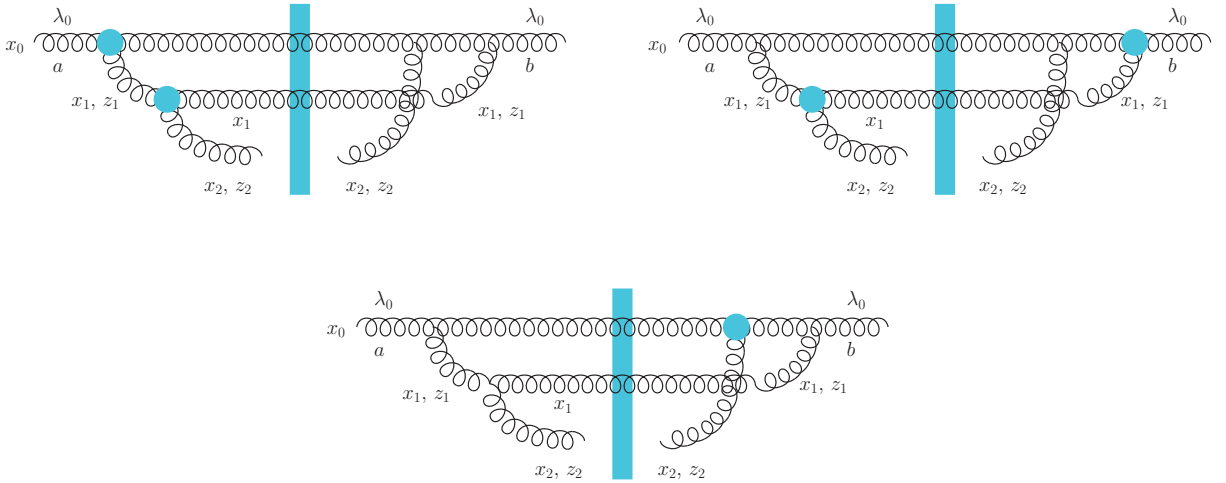


FIG. 9. Examples of non-ladder gluon diagrams. Non-eikonal gluon emission vertices are again denoted by shaded circles.

The situation with the non-ladder gluon diagrams is not so straightforward. Examples of the non-ladder gluon graphs are shown in Fig. 9. While the topology of all three diagrams in Fig. 9 is the same, the three graphs represent all possible contributions coming from the non-eikonal spin-transferring vertices. For $1 \gg z_1 \gg z_2$ the longitudinal integrals in Fig. 9 are also given by Eq. (40) and are logarithmic, generating two logarithms of energy when convoluted with $\sim 1/(z_2 s)$ initial conditions. The transverse coordinate and polarization dependence of the diagrams in Fig. 9 can be obtained similarly to the above calculation for the non-ladder quark graphs. We get (after doing some algebra)

$$A = B = C \propto \lambda_0 \int \frac{d^2 x_1 d^2 x_2}{x_{10}^2 x_{21}^2 x_{20}^2} \underline{x}_{21} \cdot \underline{x}_{20} \theta(x_{10}^2 z_1 - \max\{x_{21}^2, x_{20}^2\} z_2). \tag{43}$$

The origin of the θ -function in Eq. (43) is as follows. Imposing the ordering (38) onto the diagrams in Fig. 9 yields $x_{21}^2 z_2 \ll x_{10}^2 z_1$ to the left of the shock wave and $x_{20}^2 z_2 \ll x_{10}^2 z_1$ to the right of the shock wave. To satisfy both conditions we require

$$x_{10}^2 z_1 \gg \max \{x_{21}^2, x_{20}^2\} z_2, \quad (44)$$

which is imposed via the θ -function in Eq. (43). The logarithmic part of the x_2 -integral in Eq. (43) comes from the IR region where $x_{21} \sim x_{20} \gg x_{10}$, similar to Eqs. (41) and (42). In that region we get

$$A = B = C \propto \lambda_0 \pi^2 \int_{1/(z_1 s)} \frac{dx_{10}^2}{x_{10}^2} \int_{x_{10}^2}^{x_{10}^2 z_1/z_2} \frac{dx_{21}^2}{x_{21}^2}, \quad (45)$$

thus generating two logarithms of energy from the transverse integration as well.

We see that the non-ladder gluon graphs in Fig. 9 are DLA diagrams. Moreover, unlike the non-ladder quark graphs in Fig. 8, the non-ladder gluon graphs do not seem to come with diagrams which cancel them. While some cancellations do exist for certain classes of non-ladder gluon diagrams, they are far insufficient to cancel all the non-ladder gluon contributions. We conclude that to construct helicity evolution equations one has to include non-ladder gluon diagrams as well.

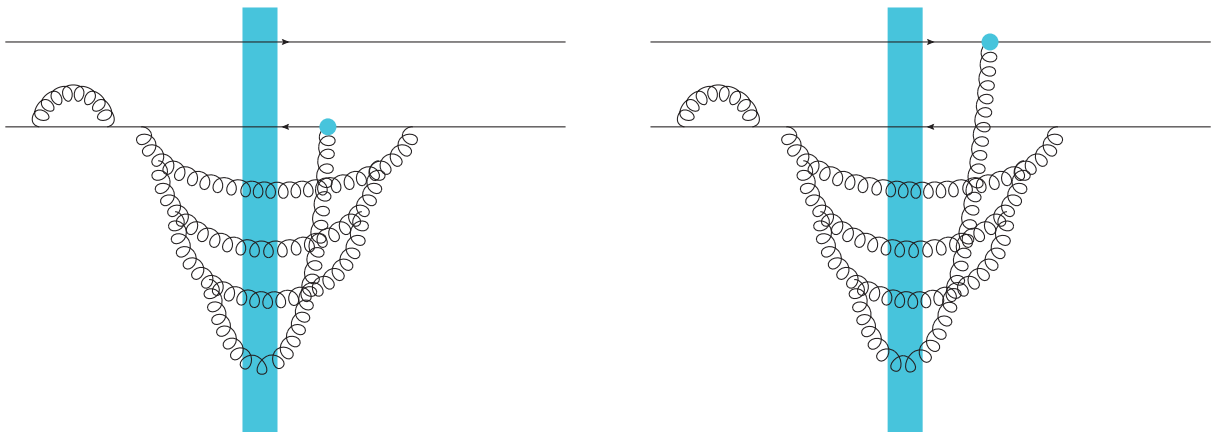


FIG. 10. Examples of non-ladder gluon diagrams with eikonal “real” and “virtual” gluons.

There is another subtlety here. Diagram C in Fig. 9, while DLA-type, contains the s -channel gluon with longitudinal momentum fraction z_1 : both the emission and absorption vertices for that gluon are eikonal. The fact that the non-ladder gluon z_2 connects in the non-eikonal way to the initial (upper-most) gluon line allowed gluon z_1 to be a “regular” eikonal gluon, just like in the unpolarized LLA evolution. This observation opens up another range of possibilities: it seems the gluons like z_1 can also be completely virtual. In addition, instead of just one eikonal gluon, we could emit (and absorb) several of them. Examples of such diagrams are depicted in Fig. 10, where we have both eikonal virtual corrections and “real” gluons (in the dipole model terminology [10–12, 75]). All such diagrams have to be included in the DLA helicity evolution.³

Let us also point out that non-ladder gluons are not always non-planar gluons, which can simply be eliminated by taking the large- N_c limit. For instance the diagram in the left panel of Fig. 10 is subleading in N_c , while diagram in the right panel is leading-order in N_c . While taking the large- N_c limit would eliminate some non-ladder diagrams, it would also leave other non-ladder diagrams almost unchanged.

To summarize this Section, let us reiterate that for DLA helicity evolution one has to include non-eikonal soft quark and gluon emissions. They may lead to a ladder (or mixing of quark and gluon ladders), but soft gluons may also be emitted in a non-ladder way. In such case the unpolarized eikonal-gluon evolution may contribute “real” and “virtual” corrections as well. We are now ready to write down an equation for helicity evolution.

³ One may show that the non-ladder gluon projects the eikonal gluon evolution onto a color-octet (adjoint) channel. This appears to be similar to the unpolarized octet evolution which was employed by BER [1].

V. EVOLUTION EQUATION FOR THE POLARIZED DIPOLE OPERATOR

Consider an eikonal quark or gluon, which may interact with the target shock wave in a polarization-dependent way. The propagation of such a particle is described by either one of the following operators:

$$V_{\underline{x}} = V_{\underline{x}}^{unp} + \sigma V_{\underline{x}}^{pol}, \quad U_{\underline{x}} = U_{\underline{x}}^{unp} + \lambda U_{\underline{x}}^{pol}. \quad (46)$$

While $V_{\underline{x}}^{unp}$ and $U_{\underline{x}}^{unp}$ are the infinite light-cone Wilson line operators (8) (in the fundamental and adjoint representations respectively), $V_{\underline{x}}^{pol}$ and $U_{\underline{x}}^{pol}$ are more involved. These latter objects are Wilson lines only in the sense of eikonal propagation. They may change representation between fundamental and adjoint as eikonal quarks become eikonal gluons (by emitting softer quarks) and vice versa (but only one conversion may take place on each side of the shock wave, since we only need the leading-order sub-eikonal correction). Hence we will not write down an explicit operatorial definition for them. It is likely that one can write down the operator definitions of $V_{\underline{x}}^{pol}$ and $U_{\underline{x}}^{pol}$ along the lines of the calculation performed in [43]. For the purposes of constructing the evolution equations below we only need to know that these are eikonal quarks or gluons which may emit softer particles in the polarization-dependent way.

The polarized dipole operator is

$$\begin{aligned} \left\langle\left\langle \text{tr} \left[V_{\underline{x}} V_{\underline{y}}^\dagger(\sigma) \right] + \text{tr} \left[V_{\underline{y}}(\sigma) V_{\underline{x}}^\dagger \right] \right\rangle\right\rangle_{\Sigma}(z) &= \sigma \left\langle\left\langle \text{tr} \left[V_{\underline{x}}^{unp} V_{\underline{y}}^{pol \dagger} \right] + \text{tr} \left[V_{\underline{y}}^{pol} V_{\underline{x}}^{unp \dagger} \right] \right\rangle\right\rangle(z) \\ &= 2\sigma \left\langle\left\langle \text{Re} \left(\text{tr} \left[V_{\underline{x}}^{unp} V_{\underline{y}}^{pol \dagger} \right] \right) \right\rangle\right\rangle(z) \end{aligned} \quad (47)$$

in the fundamental representation and

$$\begin{aligned} \left\langle\left\langle \text{Tr} \left[U_{\underline{x}} U_{\underline{y}}^\dagger(\lambda) \right] + \text{Tr} \left[U_{\underline{y}}(\lambda) U_{\underline{x}}^\dagger \right] \right\rangle\right\rangle_{\Sigma}(z) &= \lambda \left\langle\left\langle \text{Tr} \left[U_{\underline{x}}^{unp} U_{\underline{y}}^{pol \dagger} \right] + \text{Tr} \left[U_{\underline{y}}^{pol} U_{\underline{x}}^{unp \dagger} \right] \right\rangle\right\rangle(z) \\ &= 2\lambda \left\langle\left\langle \text{Re} \left(\text{Tr} \left[U_{\underline{x}}^{unp} U_{\underline{y}}^{pol \dagger} \right] \right) \right\rangle\right\rangle(z) \end{aligned} \quad (48)$$

in the adjoint representation. (From now on we will suppress the subscript Σ in the angle brackets: without loss of generality one may simply assume that the proton helicity is $\Sigma = +1$.) Note that since U^{pol} is not a standard adjoint Wilson line, it is not clear whether it is purely real or whether it has an imaginary part: this is why we left the Re sign in the last line of Eq. (48).

Note that it is not very probable that the gluon helicity TMD is related to the operator in Eq. (48). As the unpolarized gluon TMD in general is not related to the unpolarized adjoint dipole [30, 42–44, 76], it is likely that a proper operator governing the high-energy behavior of the gluon helicity TMD is different from (48), invoking higher-order correlators such as the quadrupole. Here we consider this operator simply because it will help us write a closed system of evolution equations in the large- N_c & N_f case.

Below we will also sometimes employ the doublet

$$W_{\underline{x}\underline{y}}^{pol}(z) \equiv \begin{pmatrix} \frac{1}{N_c} \left\langle\left\langle \text{tr} \left[V_{\underline{x}}^{unp} V_{\underline{y}}^{pol \dagger} \right] + \text{tr} \left[V_{\underline{y}}^{pol} V_{\underline{x}}^{unp \dagger} \right] \right\rangle\right\rangle(z) \\ \frac{1}{N_c^2 - 1} \left\langle\left\langle \text{Tr} \left[U_{\underline{x}}^{unp} U_{\underline{y}}^{pol \dagger} \right] + \text{Tr} \left[U_{\underline{y}}^{pol} U_{\underline{x}}^{unp \dagger} \right] \right\rangle\right\rangle(z) \end{pmatrix}. \quad (49)$$

A. Quark Dipole Evolution

We begin with the fundamental dipole. To write an operator evolution equation (similar to the first equation in the Balitsky hierarchy [13, 14]), we have to perform one step of evolution, which is shown in Fig. 11. Here we depict an equation only for the first out of the two traces in Eq. (47): however, it should be stressed that the resulting equations are only valid when the trace is part of the whole polarized dipole operator (47), that is, when both traces are added together.

The first two diagrams on the right-hand side of the first row and the diagram in the second row can be used to construct the ladder approximation. The last two diagrams in the first row are the non-ladder graphs. The last three rows consist of the usual unpolarized small- x evolution (of the BK/JIMWLK type) which also contributes to the DLA as we have seen in Figs. 10 and 9.

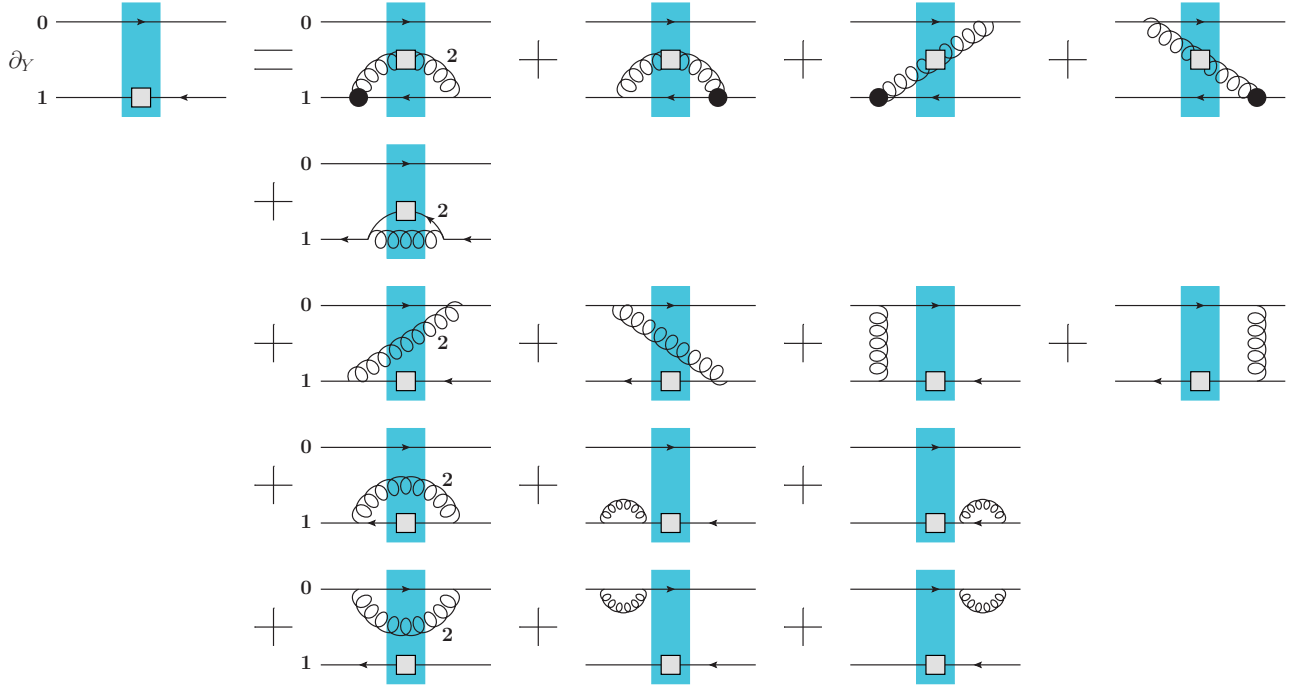


FIG. 11. One step of the polarized fundamental dipole evolution. Shaded rectangles denote the shock wave. Black circles represent spin-dependent (sub-eikonal) soft gluon emission vertices. Gray squares denote the lines carrying polarization information.

Adding up the contributions of all the diagrams on the right hand side of Eq. (11) yields the following evolution equation for the fundamental polarized dipole:

$$\begin{aligned}
\frac{1}{N_c} \langle \text{tr} [V_{\underline{0}}^{unp} V_{\underline{1}}^{pol \dagger}] \rangle(z) &= \frac{1}{N_c} \langle \text{tr} [V_{\underline{0}}^{unp} V_{\underline{1}}^{pol \dagger}] \rangle_0(z) + \frac{\alpha_s}{2\pi^2} \int_{z_i}^z \frac{dz'}{z} \int_{\rho'^2} d^2 x_2 \\
&\times \left[\left(\frac{1}{x_{21}^2} \theta(x_{10}^2 z - x_{21}^2 z') - \frac{x_{21} \cdot x_{20}}{x_{21}^2 x_{20}^2} \theta(x_{10}^2 z - \max\{x_{21}^2, x_{20}^2\} z') \right) \frac{2}{N_c} \langle \text{tr} [t^b V_{\underline{0}}^{unp} t^a V_{\underline{1}}^{unp \dagger}] U_{\underline{2}}^{pol ba} \rangle(z') \right. \\
&+ \left. \frac{1}{x_{21}^2} \theta(x_{10}^2 z - x_{21}^2 z') \frac{1}{N_c} \langle \text{tr} [t^b V_{\underline{0}}^{unp} t^a V_{\underline{2}}^{pol \dagger}] U_{\underline{1}}^{unp ba} \rangle(z') \right] \\
&+ \frac{\alpha_s}{\pi^2} \int_{z_i}^z \frac{dz'}{z'} \int_{\rho'^2} d^2 x_2 \frac{x_{10}^2}{x_{21}^2 x_{20}^2} \theta(x_{10}^2 z - x_{21}^2 z') \frac{1}{N_c} \left[\langle \text{tr} [t^b V_{\underline{0}}^{unp} t^a V_{\underline{1}}^{pol \dagger}] U_{\underline{2}}^{unp ba} \rangle(z') - C_F \langle \text{tr} [V_{\underline{0}}^{unp} V_{\underline{1}}^{pol \dagger}] \rangle(z') \right].
\end{aligned} \tag{50}$$

The coordinates used above are explained in Fig. 11: we use an abbreviated notation, e.g. $V_{\underline{0}}$ stands for V_{x_0} . The terms on the right of Eq. (50) correspond to the diagrams on the right of Fig. 11. Namely, the first two lines of Eq. (50) correspond to the first row of Fig. 11. The θ -functions define the range of x_2 -integration giving the DLA contribution, while $\rho'^2 = 1/(z's)$ is the UV cutoff. The argument z' denotes the light-cone momentum fraction of the softest (polarized or unpolarized) Wilson line operator in the correlator. Note that the UV cutoff “evolves” with z' . The third line of Eq. (50) corresponds to the second row of Fig. 11. Finally, the last line of Eq. (50) represents the last three rows of Fig. 11. The $\langle \dots \rangle_0$ term on the right of Eq. (50) represents initial conditions for the evolution, which, for simplicity, are not shown in Fig. 11.

To further simplify Eq. (50) we note that with the DLA accuracy (remembering that $z \geq z'$, see (45))

$$\frac{1}{x_{21}^2} \theta(x_{10}^2 z - x_{21}^2 z') - \frac{x_{21} \cdot x_{20}}{x_{21}^2 x_{20}^2} \theta(x_{10}^2 z - \max\{x_{21}^2, x_{20}^2\} z') \approx \frac{1}{x_{21}^2} \theta(x_{10} - x_{21}). \tag{51}$$

Note that since

$$U_{\underline{2}}^{unp ba} = 2 \text{tr} [t^a V_{\underline{2}}^{unp} t^b V_{\underline{2}}^{unp \dagger}] \tag{52}$$

one can use Fierz identity to show that

$$2 \operatorname{tr} \left[t^b V_{\underline{0}}^{unp} t^a V_{\underline{1}}^{pol \dagger} \right] U_{\underline{2}}^{unp \ ba} = \operatorname{tr} \left[V_{\underline{0}}^{unp} V_{\underline{2}}^{unp \dagger} \right] \operatorname{tr} \left[V_{\underline{2}}^{unp} V_{\underline{1}}^{pol \dagger} \right] - \frac{1}{N_c} \operatorname{tr} \left[V_{\underline{0}}^{unp} V_{\underline{1}}^{pol \dagger} \right]. \quad (53)$$

Using these results in Eq. (50) yields

$$\begin{aligned} \frac{1}{N_c} \left\langle \operatorname{tr} \left[V_{\underline{0}}^{unp} V_{\underline{1}}^{pol \dagger} \right] \right\rangle (z) &= \frac{1}{N_c} \left\langle \operatorname{tr} \left[V_{\underline{0}}^{unp} V_{\underline{1}}^{pol \dagger} \right] \right\rangle_0 (z) + \frac{\alpha_s}{2\pi^2} \int_{z_i}^z \frac{dz'}{z} \int_{\rho'^2} d^2 x_2 \\ &\times \left[\frac{1}{x_{21}^2} \theta(x_{10} - x_{21}) \frac{2}{N_c} \left\langle \operatorname{tr} \left[t^b V_{\underline{0}}^{unp} t^a V_{\underline{1}}^{unp \dagger} \right] U_{\underline{2}}^{pol \ ba} \right\rangle (z') \right. \\ &+ \left. \frac{1}{x_{21}^2} \theta(x_{10}^2 z - x_{21}^2 z') \frac{1}{N_c} \left\langle \operatorname{tr} \left[t^b V_{\underline{0}}^{unp} t^a V_{\underline{2}}^{pol \dagger} \right] U_{\underline{1}}^{unp \ ba} \right\rangle (z') \right] \\ &+ \frac{\alpha_s}{2\pi^2} \int_{z_i}^z \frac{dz'}{z'} \int_{\rho'^2} d^2 x_2 \frac{x_{10}^2}{x_{21}^2 x_{20}^2} \theta(x_{10}^2 z - x_{21}^2 z') \\ &\times \frac{1}{N_c} \left[\left\langle \operatorname{tr} \left[V_{\underline{0}}^{unp} V_{\underline{2}}^{unp \dagger} \right] \operatorname{tr} \left[V_{\underline{2}}^{unp} V_{\underline{1}}^{pol \dagger} \right] \right\rangle (z') - N_c \left\langle \operatorname{tr} \left[V_{\underline{0}}^{unp} V_{\underline{1}}^{pol \dagger} \right] \right\rangle (z') \right]. \quad (54) \end{aligned}$$

At this point one can notice that the last square brackets on the right-hand side of Eq. (54) go to zero as $\underline{2} \rightarrow \underline{0}$, hence the $x_{20} \ll x_{10}$ region of integration is not logarithmic and is beyond the DLA. The only DLA contribution in the last term on the right of Eq. (54) comes from the $x_{21} \ll x_{10}$ region, where one can replace

$$\frac{x_{10}^2}{x_{21}^2 x_{20}^2} \rightarrow \frac{1}{x_{21}^2} \theta(x_{10} - x_{21}). \quad (55)$$

We obtain

$$\begin{aligned} \frac{1}{N_c} \left\langle \operatorname{tr} \left[V_{\underline{0}}^{unp} V_{\underline{1}}^{pol \dagger} \right] \right\rangle (z) &= \frac{1}{N_c} \left\langle \operatorname{tr} \left[V_{\underline{0}}^{unp} V_{\underline{1}}^{pol \dagger} \right] \right\rangle_0 (z) + \frac{\alpha_s}{2\pi^2} \int_{z_i}^z \frac{dz'}{z} \int_{\rho'^2} \frac{d^2 x_2}{x_{21}^2} \\ &\times \left\{ \theta(x_{10} - x_{21}) \frac{2}{N_c} \left\langle \operatorname{tr} \left[t^b V_{\underline{0}}^{unp} t^a V_{\underline{1}}^{unp \dagger} \right] U_{\underline{2}}^{pol \ ba} \right\rangle (z') + \theta(x_{10}^2 z - x_{21}^2 z') \frac{1}{N_c} \left\langle \operatorname{tr} \left[t^b V_{\underline{0}}^{unp} t^a V_{\underline{2}}^{pol \dagger} \right] U_{\underline{1}}^{unp \ ba} \right\rangle (z') \right. \\ &+ \left. \frac{z}{z'} \theta(x_{10} - x_{21}) \frac{1}{N_c} \left[\left\langle \operatorname{tr} \left[V_{\underline{0}}^{unp} V_{\underline{2}}^{unp \dagger} \right] \operatorname{tr} \left[V_{\underline{2}}^{unp} V_{\underline{1}}^{pol \dagger} \right] \right\rangle (z') - N_c \left\langle \operatorname{tr} \left[V_{\underline{0}}^{unp} V_{\underline{1}}^{pol \dagger} \right] \right\rangle (z') \right] \right\}. \quad (56) \end{aligned}$$

Finally, to cast Eq. (56) in an explicitly DLA form we redefine matrix elements in it using Eq. (10) (cf. Eq. (42) in [67]). Note that z , used in the rescaling Eq. (10), is not always the smallest longitudinal momentum fraction in a diagram (and hence is not always in the argument of the matrix elements). For instance, the operators in the last line of Eq. (56) have the polarized line carrying momentum fraction z , while the softest unpolarized Wilson line carries the momentum fraction z' , which enters in the argument of the matrix elements. Using the redefinition (10) (and keeping in mind that the z -rescaling is determined by the polarized line, not necessarily by the softest parton which determines the argument of the Wilson line matrix element) we obtain

$$\begin{aligned} \frac{1}{N_c} \left\langle \left\langle \operatorname{tr} \left[V_{\underline{0}}^{unp} V_{\underline{1}}^{pol \dagger} \right] \right\rangle \right\rangle (z) &= \frac{1}{N_c} \left\langle \left\langle \operatorname{tr} \left[V_{\underline{0}}^{unp} V_{\underline{1}}^{pol \dagger} \right] \right\rangle \right\rangle_0 (z) + \frac{\alpha_s}{2\pi^2} \int_{z_i}^z \frac{dz'}{z'} \int_{\rho'^2} \frac{d^2 x_2}{x_{21}^2} \\ &\times \left\{ \theta(x_{10} - x_{21}) \frac{2}{N_c} \left\langle \left\langle \operatorname{tr} \left[t^b V_{\underline{0}}^{unp} t^a V_{\underline{1}}^{unp \dagger} \right] U_{\underline{2}}^{pol \ ba} \right\rangle \right\rangle (z') + \theta(x_{10}^2 z - x_{21}^2 z') \frac{1}{N_c} \left\langle \left\langle \operatorname{tr} \left[t^b V_{\underline{0}}^{unp} t^a V_{\underline{2}}^{pol \dagger} \right] U_{\underline{1}}^{unp \ ba} \right\rangle \right\rangle (z') \right. \\ &+ \left. \theta(x_{10} - x_{21}) \frac{1}{N_c} \left[\left\langle \left\langle \operatorname{tr} \left[V_{\underline{0}}^{unp} V_{\underline{2}}^{unp \dagger} \right] \operatorname{tr} \left[V_{\underline{2}}^{unp} V_{\underline{1}}^{pol \dagger} \right] \right\rangle \right\rangle (z') - N_c \left\langle \left\langle \operatorname{tr} \left[V_{\underline{0}}^{unp} V_{\underline{1}}^{pol \dagger} \right] \right\rangle \right\rangle (z') \right] \right\}. \quad (57) \end{aligned}$$

This is the simplest form of the evolution equation for the fundamental dipole we could obtain without making any additional assumptions. Note that Eq. (52), and hence the identity (53), would not be valid if we replace $U_{\underline{2}}^{unp}$ in them with $U_{\underline{2}}^{pol}$, since it is not a standard Wilson line.

We would like to stress once again that Eq. (57) is only valid if the operator on its left hand side is considered as a part (a ‘‘half’’) of the polarized dipole operator (47). The corresponding equation for the full polarized fundamental dipole operator (47) is

$$\begin{aligned}
& \frac{1}{N_c} \left\langle \left\langle \text{tr} \left[V_{\underline{0}}^{unp} V_{\underline{1}}^{pol \dagger} \right] + \text{tr} \left[V_{\underline{1}}^{pol} V_{\underline{0}}^{unp \dagger} \right] \right\rangle \right\rangle (z) = \frac{1}{N_c} \left\langle \left\langle \text{tr} \left[V_{\underline{0}}^{unp} V_{\underline{1}}^{pol \dagger} \right] + \text{tr} \left[V_{\underline{1}}^{pol} V_{\underline{0}}^{unp \dagger} \right] \right\rangle \right\rangle_0 (z) + \frac{\alpha_s}{2\pi^2} \int_{z_i}^z \frac{dz'}{z'} \int_{\rho'^2} d^2 x_2 \\
& \times \left\{ \theta(x_{10} - x_{21}) \frac{2}{N_c} \left\langle \left\langle \text{tr} \left[t^b V_{\underline{0}}^{unp} t^a V_{\underline{1}}^{unp \dagger} \right] U_{\underline{2}}^{pol ba} + \text{tr} \left[t^b V_{\underline{1}}^{unp} t^a V_{\underline{0}}^{unp \dagger} \right] U_{\underline{2}}^{pol \dagger ba} \right\rangle \right\rangle (z') \right. \\
& + \theta(x_{10}^2 z - x_{21}^2 z') \frac{1}{N_c} \left\langle \left\langle \text{tr} \left[t^b V_{\underline{0}}^{unp} t^a V_{\underline{2}}^{pol \dagger} \right] U_{\underline{1}}^{unp ba} + \text{tr} \left[t^b V_{\underline{2}}^{pol} t^a V_{\underline{0}}^{unp \dagger} \right] U_{\underline{1}}^{unp \dagger ba} \right\rangle \right\rangle (z') \\
& + \theta(x_{10} - x_{21}) \frac{1}{N_c} \left[\left\langle \left\langle \text{tr} \left[V_{\underline{0}}^{unp} V_{\underline{2}}^{unp \dagger} \right] \text{tr} \left[V_{\underline{2}}^{unp} V_{\underline{1}}^{pol \dagger} \right] + \text{tr} \left[V_{\underline{2}}^{unp} V_{\underline{0}}^{unp \dagger} \right] \text{tr} \left[V_{\underline{1}}^{pol} V_{\underline{2}}^{unp \dagger} \right] \right\rangle \right\rangle (z') \right. \\
& \left. - N_c \left\langle \left\langle \text{tr} \left[V_{\underline{0}}^{unp} V_{\underline{1}}^{pol \dagger} \right] + \text{tr} \left[V_{\underline{1}}^{pol} V_{\underline{0}}^{unp \dagger} \right] \right\rangle \right\rangle (z') \right\}. \tag{58}
\end{aligned}$$

B. Gluon Dipole

Similar to the above, we can construct the evolution equation for the polarized gluon dipole. Instead of Eq. (50) we get

$$\begin{aligned}
& \frac{1}{N_c^2 - 1} \left\langle \text{Tr} \left[U_{\underline{0}}^{unp} U_{\underline{1}}^{pol \dagger} \right] \right\rangle (z) = \frac{1}{N_c^2 - 1} \left\langle \text{Tr} \left[U_{\underline{0}}^{unp} U_{\underline{1}}^{pol \dagger} \right] \right\rangle_0 (z) + \frac{\alpha_s}{2\pi^2} \int_{z_i}^z \frac{dz'}{z'} \int d^2 x_2 \\
& \times \left[\left(\frac{1}{x_{21}^2} \theta(x_{10}^2 z - x_{21}^2 z') - \frac{x_{21} \cdot x_{20}}{x_{21}^2 x_{20}^2} \theta(x_{10}^2 z - \max\{x_{21}^2, x_{20}^2\} z') \right) \right. \\
& \times \frac{4}{N_c^2 - 1} \left\langle \text{Tr} \left[T^b U_{\underline{0}}^{unp} T^a U_{\underline{1}}^{unp \dagger} \right] U_{\underline{2}}^{pol ba} \right\rangle (z') \\
& \left. - \frac{1}{x_{21}^2} \theta(x_{10}^2 z - x_{21}^2 z') \frac{N_f}{N_c^2 - 1} \left\langle \text{tr} \left[t^b V_{\underline{1}}^{unp} t^a V_{\underline{2}}^{pol \dagger} \right] U_{\underline{0}}^{unp ba} + \text{tr} \left[t^b V_{\underline{2}}^{pol} t^a V_{\underline{1}}^{unp \dagger} \right] U_{\underline{0}}^{unp ba} \right\rangle (z') \right] \\
& + \frac{\alpha_s}{\pi^2} \int_{z_i}^z \frac{dz'}{z'} \int_{\rho'^2} d^2 x_2 \frac{x_{10}^2}{x_{21}^2 x_{20}^2} \theta(x_{10}^2 z - x_{21}^2 z') \\
& \times \frac{1}{N_c^2 - 1} \left[\left\langle \text{Tr} \left[T^b U_{\underline{0}}^{unp} T^a U_{\underline{1}}^{pol \dagger} \right] U_{\underline{2}}^{unp ba} \right\rangle (z') - N_c \left\langle \text{Tr} \left[U_{\underline{0}}^{unp} U_{\underline{1}}^{pol \dagger} \right] \right\rangle (z') \right]. \tag{59}
\end{aligned}$$

Note that t^a and T^a are the fundamental and adjoint $SU(N_c)$ generators correspondingly, with tr denoting the fundamental traces and Tr denoting the adjoint ones. Equation (59) is illustrated in Fig. 12, where again we omit showing the initial conditions term.

We can further simplify Eq. (59) along the above lines. Instead of Eq. (53) resulting from the Fierz identity, now we have

$$\text{Tr} \left[T^b U_{\underline{0}}^{unp} T^a U_{\underline{1}}^{pol \dagger} \right] U_{\underline{2}}^{unp ba} = \text{Tr} \left[T^a U_{\underline{2}}^{unp} U_{\underline{0}}^{unp \dagger} T^a U_{\underline{0}}^{unp} U_{\underline{1}}^{pol \dagger} \right], \tag{60}$$

which can be used to justify the substitution (55) (that is, only the region $x_{21} \ll x_{10}$ is logarithmic). Using Eqs. (51) and (55) in Eq. (59) yields

$$\begin{aligned}
& \frac{1}{N_c^2 - 1} \left\langle \text{Tr} \left[U_{\underline{0}}^{unp} U_{\underline{1}}^{pol \dagger} \right] \right\rangle (z) = \frac{1}{N_c^2 - 1} \left\langle \text{Tr} \left[U_{\underline{0}}^{unp} U_{\underline{1}}^{pol \dagger} \right] \right\rangle_0 (z) + \frac{\alpha_s}{2\pi^2} \int_{z_i}^z \frac{dz'}{z'} \int_{\rho'^2} d^2 x_2 \\
& \times \left\{ \theta(x_{10} - x_{21}) \frac{4}{N_c^2 - 1} \left\langle \text{Tr} \left[T^b U_{\underline{0}}^{unp} T^a U_{\underline{1}}^{unp \dagger} \right] U_{\underline{2}}^{pol ba} \right\rangle (z') \right. \\
& - \theta(x_{10}^2 z - x_{21}^2 z') \frac{N_f}{N_c^2 - 1} \left\langle \text{tr} \left[t^b V_{\underline{1}}^{unp} t^a V_{\underline{2}}^{pol \dagger} \right] U_{\underline{0}}^{unp ba} + \text{tr} \left[t^b V_{\underline{2}}^{pol} t^a V_{\underline{1}}^{unp \dagger} \right] U_{\underline{0}}^{unp ba} \right\rangle (z') \\
& \left. + \frac{z}{z'} \theta(x_{10} - x_{21}) \frac{2}{N_c^2 - 1} \left[\left\langle \text{Tr} \left[T^b U_{\underline{0}}^{unp} T^a U_{\underline{1}}^{pol \dagger} \right] U_{\underline{2}}^{unp ba} \right\rangle (z') - N_c \left\langle \text{Tr} \left[U_{\underline{0}}^{unp} U_{\underline{1}}^{pol \dagger} \right] \right\rangle (z') \right] \right\}. \tag{61}
\end{aligned}$$

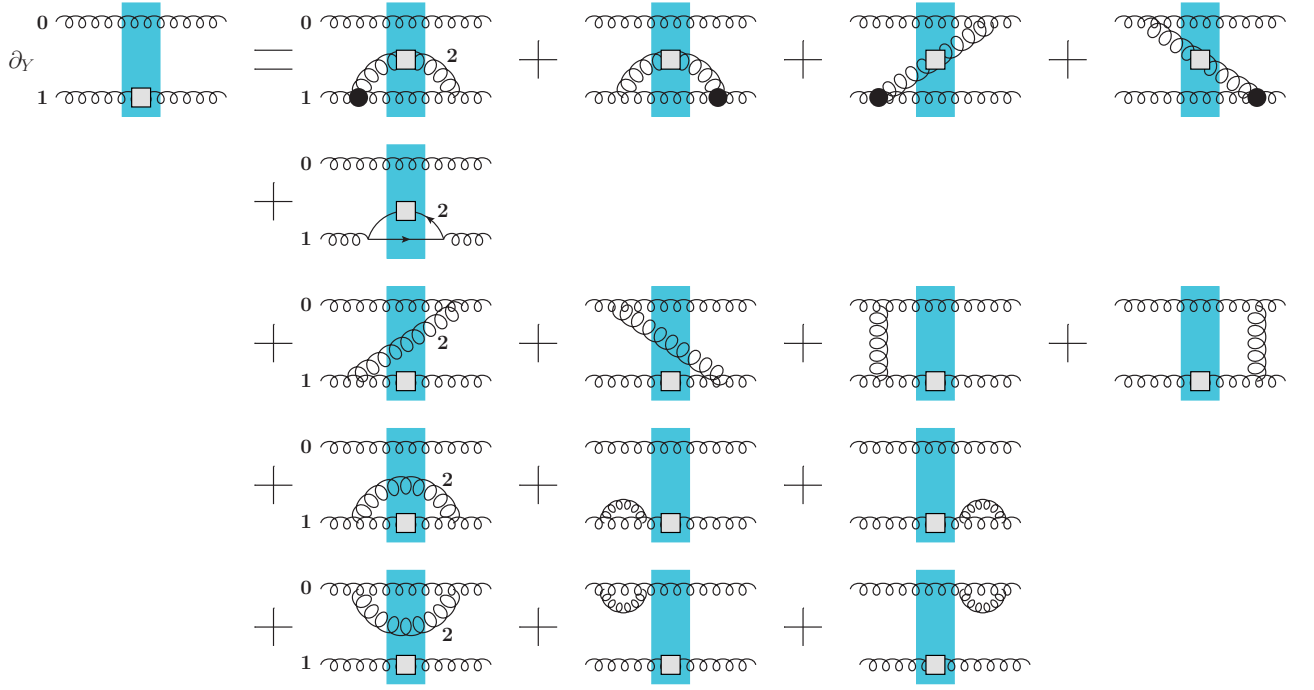


FIG. 12. One step of the polarized adjoint dipole evolution. Shaded rectangles denote the shock wave. Black circles represent spin-dependent (sub-eikonal) soft gluon emission vertices. Gray squares denote the lines carrying polarization information.

Finally, performing the redefinition (10) we arrive at

$$\begin{aligned}
\frac{1}{N_c^2 - 1} \left\langle\left\langle \text{Tr} \left[U_{\underline{0}}^{unp} U_{\underline{1}}^{pol \dagger} \right] \right\rangle\right\rangle (z) &= \frac{1}{N_c^2 - 1} \left\langle\left\langle \text{Tr} \left[U_{\underline{0}}^{unp} U_{\underline{1}}^{pol \dagger} \right] \right\rangle\right\rangle_0 (z) + \frac{\alpha_s}{2\pi^2} \int_{z_i}^z \frac{dz'}{z} \int \frac{d^2 x_2}{x_{21}^2} \\
&\times \left\{ \theta(x_{10} - x_{21}) \frac{4}{N_c^2 - 1} \left\langle\left\langle \text{Tr} \left[T^b U_{\underline{0}}^{unp} T^a U_{\underline{1}}^{unp \dagger} \right] U_{\underline{2}}^{pol ba} \right\rangle\right\rangle (z') \right. \\
&- \theta(x_{10}^2 z - x_{21}^2 z') \frac{N_f}{N_c^2 - 1} \left\langle\left\langle \text{tr} \left[t^b V_{\underline{1}}^{unp} t^a V_{\underline{2}}^{pol \dagger} \right] U_{\underline{0}}^{unp ba} + \text{tr} \left[t^b V_{\underline{2}}^{pol} t^a V_{\underline{1}}^{unp \dagger} \right] U_{\underline{0}}^{unp ba} \right\rangle\right\rangle (z') \\
&\left. + \theta(x_{10} - x_{21}) \frac{2}{N_c^2 - 1} \left[\left\langle\left\langle \text{Tr} \left[T^b U_{\underline{0}}^{unp} T^a U_{\underline{1}}^{pol \dagger} \right] U_{\underline{2}}^{unp ba} \right\rangle\right\rangle (z') - N_c \left\langle\left\langle \text{Tr} \left[U_{\underline{0}}^{unp} U_{\underline{1}}^{pol \dagger} \right] \right\rangle\right\rangle (z') \right] \right\}. \quad (62)
\end{aligned}$$

The evolution equation for the full adjoint polarized dipole (48) can be constructed by adding to Eq. (62) its hermitean conjugate, similar to the fundamental dipole case.

Equations (58) and (62) are our main equations. Unfortunately they are not closed, like the equations in the Balitsky hierarchy. That is, the objects (operator expectation values) on their right-hand sides are not always the same as the polarized dipole operators on their left-hand sides: hence, similar to JIMWLK equation, they can only be solved by functional methods [77, 78].

C. Ladder Approximation

We would now like to cross check our results against those of BER [1]. This is no easy task given that at the moment we do not have a solution of Eqs. (58) and (62) and that our rapidity evolution method is very different from the infrared cutoff evolution employed by BER. In addition, no analytic solution for the DLA $g_1(x, Q^2)$ evolution was derived in [1], although an approximate expression was found in [79]. However, it appears possible to identify ladder diagrams both in the BER approach and in our calculation: comparing the two would provide us at least with one cross check. Certainly, an agreement between the two approaches in the ladder approximation does not yet mean a complete agreement of the two calculations. Still, the ladder cross check is a necessary condition which has to be satisfied in order to achieve this full agreement.

As was already noted by BER [1, 66], ladder diagrams are not the only ones contributing to helicity evolution. Therefore, approximating the evolution by ladder graphs is not justified. Still it may serve as a consistency check of our calculations.

With that in mind, let us put all unpolarized Wilson lines to unity, that is put all $U^{unp} = \mathbb{1}$ and $V^{unp} = \mathbb{1}$ in Eqs. (50) and (59). In addition we need to discard the contributions of the non-ladder gluons and quasi-LLA gluons: that is, we only keep the contributions of the first two diagrams in the first line and the diagram in the second line of Figs. 11 and 12. We then get

$$\begin{aligned} \frac{1}{N_c} \langle \text{tr} [V_{\underline{1}}^{pol \dagger}] \rangle (z) &= \frac{1}{N_c} \langle \text{tr} [V_{\underline{1}}^{pol \dagger}] \rangle_0 (z) + \frac{\alpha_s}{2\pi^2} \int_{z_i}^z \frac{dz'}{z} \int_{\rho^2} \frac{d^2 x_2}{x_{21}^2} \theta(x_{10}^2 z - x_{21}^2 z') \\ &\times \left[C_F \frac{1}{N_c} \langle \text{tr} [V_{\underline{2}}^{pol \dagger}] \rangle (z') + 2 C_F \frac{1}{N_c^2 - 1} \langle \text{Tr} [U_{\underline{2}}^{pol}] \rangle (z') \right], \end{aligned} \quad (63a)$$

$$\begin{aligned} \frac{1}{N_c^2 - 1} \langle \text{Tr} [U_{\underline{1}}^{pol \dagger}] \rangle (z) &= \frac{\alpha_s}{2\pi^2} \int_{z_i}^z \frac{dz'}{z} \int_{\rho^2} \frac{d^2 x_2}{x_{21}^2} \theta(x_{10}^2 z - x_{21}^2 z') \\ &\times \left[4 N_c \frac{1}{N_c^2 - 1} \langle \text{Tr} [U_{\underline{2}}^{pol}] \rangle (z') - \frac{N_f}{2 N_c} \langle \text{tr} [V_{\underline{2}}^{pol \dagger}] + \text{tr} [V_{\underline{1}}^{unp \dagger}] \rangle (z') \right]. \end{aligned} \quad (63b)$$

In the same approximation the doublet (49) becomes

$$W_{\underline{x}\underline{y}}^{pol} = \begin{pmatrix} \frac{1}{N_c} \langle \langle \text{tr} [V_{\underline{x}}^{pol}] + \text{tr} [V_{\underline{x}}^{pol \dagger}] \rangle \rangle \\ \frac{1}{N_c^2 - 1} \langle \langle \text{Tr} [U_{\underline{x}}^{pol}] + \text{Tr} [U_{\underline{x}}^{pol \dagger}] \rangle \rangle \end{pmatrix}. \quad (64)$$

In terms of the doublet Eqs. (63) become

$$W_{\underline{1}\underline{0}}^{pol}(z) = W_{\underline{1}\underline{0}}^{(0)pol}(z) + \frac{\alpha_s}{2\pi} \int_{z_i}^z \frac{dz'}{z'} \int_{\rho^2}^{x_{01}^2 z/z'} \frac{dx_{21}^2}{x_{21}^2} M W_{\underline{2}\underline{1}}^{pol}(z'), \quad (65)$$

where we have defined

$$M \equiv \begin{pmatrix} C_F & 2 C_F \\ -N_f & 4 N_c \end{pmatrix} \quad (66)$$

in agreement with Eq. (2.28) from [1]. This completes the cross-check between the ladder limits of BER and of our calculations.

One may worry that, because the calculation of BER was done in Feynman gauge but our calculation has been done in the $A^+ = 0$ light-cone gauge, the ‘‘ladder graphs’’ in the two cases may correspond to different contributions. However, a direct calculation of the ladder diagrams in these two gauges shows that they coincide. This occurs because, in the light-cone gauge, all the evolution takes place within the projectile wave function; for instance, the familiar DGLAP evolution can also be re-derived within the same framework [26].

We can solve Eq. (65) to find the intercept in the ladder case. We can look for the solution of Eq. (65) as a double Mellin transform

$$W_{\underline{1}\underline{0}}^{pol}(z) = \int \frac{d\omega}{2\pi i} \frac{d\lambda}{2\pi i} \left(\frac{z}{z_i} \right)^\omega \left(\frac{x_{01}^2}{\rho^2} \right)^\lambda W_{\omega\lambda}^{pol} \quad (67)$$

where ω and λ integrals run along straight lines parallel to the imaginary axis, $\rho^2 = 1/(zs)$ and $z_i = \Lambda^2/s$. Substituting this into Eq. (65) we obtain its solution

$$W_{\underline{1}\underline{0}}^{pol}(z) = \int \frac{d\omega}{2\pi i} \frac{d\lambda}{2\pi i} \left(\frac{z}{z_i} \right)^\omega \left(\frac{x_{01}^2}{\rho^2} \right)^\lambda \left[1 - \frac{\alpha_s}{2\pi} M \frac{1}{\omega\lambda} \right]^{-1} W_{\omega\lambda}^{pol(0)}. \quad (68)$$

The high-energy asymptotics of $W_{\underline{1}\underline{0}}^{pol}(z)$ are dominated by the rightmost pole in ω of the integrand in Eq. (68). The pole position is given by the zeroes of the determinant of the matrix in the square brackets. The poles are at

$$\omega_{\pm}(\lambda) = \frac{\alpha_s}{8\pi\lambda} \left[9N_c - \frac{1}{N_c} \pm \frac{1}{N_c} \sqrt{(1 + 7N_c^2)^2 + 16N_c N_f (1 - N_c^2)} \right]. \quad (69)$$

Clearly $\omega_+(\lambda)$ is larger for positive λ and gives the high-energy asymptotics. Note that the energy dependence comes into the integrand of (68) as $(z s)^{\lambda+\omega_\pm(\lambda)}$. Picking up the $\omega_+(\lambda)$ pole and evaluating the remaining λ -integral using the saddle-point method we find the (positive- λ) saddle point at

$$\lambda_{s.p.} = \sqrt{\frac{\alpha_s}{8\pi N_c}} \sqrt{9 N_c^2 - 1 + \sqrt{(1 + 7 N_c^2)^2 + 16 N_c N_f (1 - N_c^2)}}. \quad (70)$$

Substituting Eq. (70) into Eq. (69) yields

$$\tilde{\omega}_+(\lambda_{s.p.}) \equiv \lambda_{s.p.} + \omega_+(\lambda_{s.p.}) = \sqrt{\frac{\alpha_s}{2\pi N_c}} \sqrt{9 N_c^2 - 1 + \sqrt{(1 + 7 N_c^2)^2 + 16 N_c N_f (1 - N_c^2)}}. \quad (71)$$

The high-energy asymptotics in the ladder limit is

$$\Delta q(x, Q^2) \sim g_{1L}(x, k_T) \sim \left(\frac{1}{x}\right)^{\tilde{\omega}_+(\lambda_{s.p.})}. \quad (72)$$

Following BER we use $\alpha_s = 0.18$ and $N_f = 4$ along with $N_c = 3$ to obtain $\tilde{\omega}_+(\lambda_{s.p.}) \approx 1.12$, in agreement with the BER formula at the end of the paragraph following Eq. (4.19) in [1]. Using $\tilde{\omega}_+(\lambda_{s.p.}) \approx 1.12$ in Eq. (72) yields

$$\Delta q(x, Q^2) \sim g_{1L}(x, k_T) \sim \left(\frac{1}{x}\right)^{1.12}, \quad (73)$$

which is a slow but robust growth of the helicity TMDs and polarized PDFs with decreasing x , which may enable the low- x region to significantly contribute to $S_q(Q^2)$ from Eq. (2) and, therefore, to the helicity sum rule (1).

For a more realistic $\alpha_s = 0.3$ and $N_c = N_f = 3$ (say, for RHIC experimental kinematics) we get

$$\Delta q(x, Q^2) \sim g_{1L}(x, k_T) \sim \left(\frac{1}{x}\right)^{1.46}, \quad (74)$$

which is a very fast growth with decreasing x .

Here we have to remember that the ladder approximation used in this Subsection is not a systematic physical approximation, but rather is just a “by hand” truncation of the full calculation. Therefore, the numbers obtained in Eqs. (73) and (74), while encouraging, cannot be used to conclude that there is a significant amount of spin at small x .

D. Large- N_c Limit

By analogy with the unpolarized small- x evolution, let us try to produce a closed evolution equation out of Eq. (58) by using the large- N_c approximation. Let us point out from the outset, that the large- N_c limit is far less precise in the helicity DLA evolution at hand than it was in the unpolarized LLA small- x evolution. As is apparent from Eq. (63b), gluon splitting into a $q\bar{q}$ pair is N_c -suppressed, but is N_f -enhanced, such that it comes in with a relative “suppression factor” of N_f/N_c . In phenomenological applications with $N_f = 3$ or $N_f = 4$ this “suppression factor” is 1 or 4/3 respectively, and leads to no suppression. This is in contrast to the case of unpolarized BFKL/BK/JIMWLK evolution, where quark bubbles enter only at NLO and are easily resumable [80–83]. The leading-order in unpolarized evolution involves gluons only, such that the large- N_c limit is accurate up to order- $1/N_c^2$ corrections (see [78, 84] for more on this issue). Hence the large- N_c limit of the DLA helicity evolution we will take below should be considered with caution and one has to be very careful in interpreting the resulting numbers.

To take the large- N_c limit of Eq. (57) we first note that at large N_c only gluon emissions contribute. The soft quark emission from the upper left corner of Fig. 6 is only allowed for the parent quark. ($G \rightarrow q\bar{q}$ is N_c -suppressed.) If the parent particle is a “quark” in a typical dipole, which is, in reality, is simply a quark line in the large- N_c representation of gluons as $q\bar{q}$ pairs of different color, such splittings do not exist. This means such splittings are limited to the case when quark or anti-quark line of the dipole are from the original $q\bar{q}$ pair. Since, after several steps of small- x evolution at large- N_c most dipoles will be made out of gluons, it is probably safe to neglect the splitting in the upper left corner of Fig. 6. This means that we should discard “by hand” the second term in the curly brackets of Eq. (58).

The second observation we need to make is that $U_{\underline{2}}^{pol\ ba}$ is now (at large N_c) always an eikonal gluon line (that is, it does not convert into an eikonal quark). We therefore replace

$$\begin{aligned} & \left\langle \left\langle \text{tr} \left[t^b V_{\underline{0}}^{unp} t^a V_{\underline{1}}^{unp \dagger} \right] U_{\underline{2}}^{pol\ ba} \right\rangle \right\rangle \rightarrow \\ & \frac{1}{2} \left\langle \left\langle \text{tr} \left[V_{\underline{0}}^{unp} V_{\underline{2}}^{pol \dagger} \right] \right\rangle \right\rangle \left\langle \left\langle \text{tr} \left[V_{\underline{2}}^{unp} V_{\underline{1}}^{unp \dagger} \right] \right\rangle \right\rangle + \frac{1}{2} \left\langle \left\langle \text{tr} \left[V_{\underline{0}}^{unp} V_{\underline{2}}^{unp \dagger} \right] \right\rangle \right\rangle \left\langle \left\langle \text{tr} \left[V_{\underline{2}}^{pol} V_{\underline{1}}^{unp \dagger} \right] \right\rangle \right\rangle \end{aligned} \quad (75)$$

while identifying the gluon helicity λ_2 with the polarized quark and anti-quark line helicities σ_2 in the large- N_c limit. Equation (75) can be obtained by substituting Eq. (46) into Eq. (53) and by expanding the latter to the linear order in polarized Wilson lines.

Using Eq. (75) and discarding the the second term in the curly brackets of Eq. (57) yields in the large- N_c limit

$$\begin{aligned} \frac{1}{N_c} \left\langle \left\langle \text{tr} \left[V_{\underline{0}}^{unp} V_{\underline{1}}^{pol \dagger} \right] \right\rangle \right\rangle (z) &= \frac{1}{N_c} \left\langle \left\langle \text{tr} \left[V_{\underline{0}}^{unp} V_{\underline{1}}^{pol \dagger} \right] \right\rangle \right\rangle_0 (z) + \frac{\alpha_s}{2\pi^2} \int_{z_i}^z \frac{dz'}{z'} \int_{\rho'^2} \frac{d^2 x_2}{x_{21}^2} \theta(x_{10} - x_{21}) \\ &\times \left\{ \frac{1}{N_c} \left\langle \left\langle \text{tr} \left[V_{\underline{0}}^{unp} V_{\underline{2}}^{pol \dagger} \right] \right\rangle \right\rangle \left\langle \left\langle \text{tr} \left[V_{\underline{2}}^{unp} V_{\underline{1}}^{unp \dagger} \right] \right\rangle \right\rangle + \frac{1}{N_c} \left\langle \left\langle \text{tr} \left[V_{\underline{0}}^{unp} V_{\underline{2}}^{unp \dagger} \right] \right\rangle \right\rangle \left\langle \left\langle \text{tr} \left[V_{\underline{2}}^{pol} V_{\underline{1}}^{unp \dagger} \right] \right\rangle \right\rangle \right. \\ &\left. + \frac{1}{N_c} \left\langle \left\langle \text{tr} \left[V_{\underline{0}}^{unp} V_{\underline{2}}^{unp \dagger} \right] \right\rangle \right\rangle \left\langle \left\langle \text{tr} \left[V_{\underline{2}}^{unp} V_{\underline{1}}^{pol \dagger} \right] \right\rangle \right\rangle - \left\langle \left\langle \text{tr} \left[V_{\underline{0}}^{unp} V_{\underline{1}}^{pol \dagger} \right] \right\rangle \right\rangle \right\} (z'). \end{aligned} \quad (76)$$

Let us rewrite this result in terms of the polarized dipole amplitude

$$G_{10}(z) \equiv \frac{1}{2N_c} \left\langle \left\langle \text{tr} \left[V_{\underline{0}}^{unp} V_{\underline{1}}^{pol \dagger} \right] \right\rangle \right\rangle (z) + \frac{1}{2N_c} \left\langle \left\langle \text{tr} \left[V_{\underline{1}}^{pol} V_{\underline{0}}^{unp \dagger} \right] \right\rangle \right\rangle (z) \quad (77)$$

and the standard (albeit symmetrized) unpolarized dipole S -matrix

$$S_{01}(z) = \frac{1}{2N_c} \left\langle \left\langle \text{tr} \left[V_{\underline{0}}^{unp} V_{\underline{1}}^{unp \dagger} \right] \right\rangle \right\rangle (z) + \frac{1}{2N_c} \left\langle \left\langle \text{tr} \left[V_{\underline{1}}^{unp} V_{\underline{0}}^{unp \dagger} \right] \right\rangle \right\rangle (z) = \frac{1}{N_c} \left\langle \left\langle \text{tr} \left[V_{\underline{0}}^{unp} V_{\underline{1}}^{unp \dagger} \right] \right\rangle \right\rangle (z), \quad (78)$$

where we assumed that

$$\text{tr} \left[V_{\underline{0}}^{unp} V_{\underline{1}}^{unp \dagger} \right] = \text{tr} \left[V_{\underline{1}}^{unp} V_{\underline{0}}^{unp \dagger} \right], \quad (79)$$

which is indeed true for the unpolarized LLA evolution with leading-order (in powers of the color charge density of the target) C -even initial conditions [10–20].

Adding to Eq. (76) its hermitean conjugate with $0 \leftrightarrow 1$ we get

$$\begin{aligned} G_{10}(z) &= G_{10}^{(0)}(z) + \frac{\alpha_s N_c}{2\pi^2} \int_{z_i}^z \frac{dz'}{z'} \int_{\rho'^2} \frac{d^2 x_2}{x_{21}^2} \theta(x_{10} - x_{21}) [\Gamma_{02,21}(z') S_{21}(z') + G_{21}(z') S_{02}(z') \\ &\quad + G_{12}(z') S_{02}(z') - G_{10}(z')], \end{aligned} \quad (80)$$

where we employed the fact that Eq. (79) is valid in LLA and for standard quasi-classical initial conditions (that is, we neglected the odderon contributions).

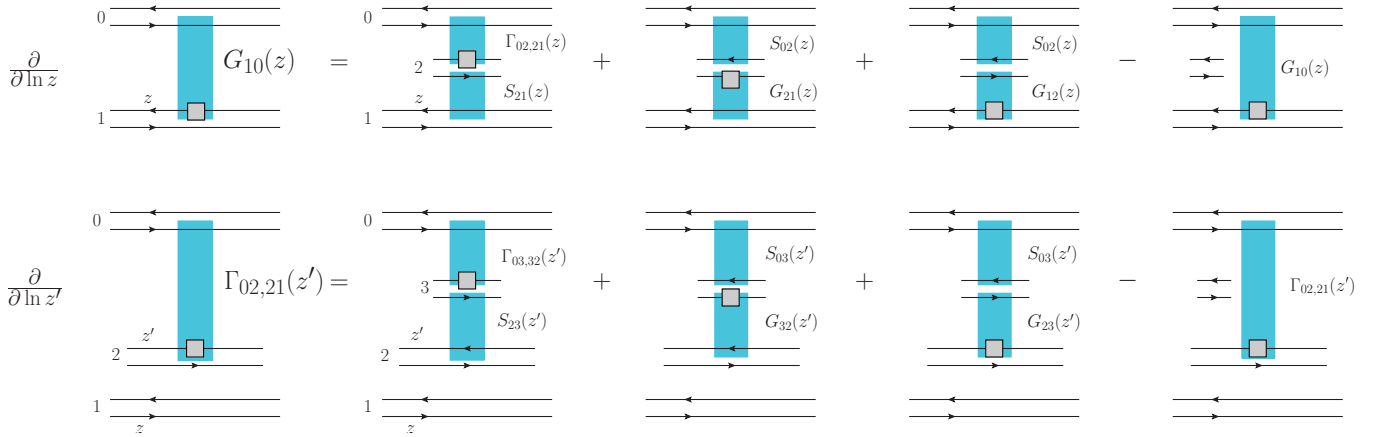


FIG. 13. Large- N_c helicity evolution for the polarized dipole amplitude G and the neighbor dipole amplitude Γ . As before, for pictorial simplicity we do not show the contributions of the initial condition terms. Double lines denote gluons at large N_c . Only one of the virtual diagrams is shown (last diagram in each line): virtual corrections to the right of the shock wave are implied, but not shown explicitly.

The evolution equation (80) is illustrated in the upper panel of Fig. 13, where the gluon lines in the large- N_c limit are represented by the double quark lines, and the lack of quark-gluon vertices denotes summation over all gluon connections from Figs. 11 and 12 [10].

Equation (80) contains a new object - the “neighbor” dipole $\Gamma_{02,21}(z')$. Note the following peculiarity of the dipole 02 formed in the first two diagrams on the right hand side of the diagrammatic evolution equation in Fig. 11: to be DLA, the subsequent evolution in that dipole has to “know” about the dipole 21. The reason for that is illustrated in Fig. 14, where, in the right panel, we show a sample diagram contributing to one step of the evolution of the dipole 02. Note that ordering (38) implies that we have to have

$$x_{21}^2 z' \gg x_{32}^2 z'' . \quad (81)$$

Just like in Eq. (80), the dipole 02 evolution is also cut off by x_{20} in the IR, $x_{32} \ll x_{20}$. We see that for $x_{20}^2 > x_{21}^2 z'/z''$ the condition (81) becomes more constraining than $x_{32} \ll x_{20}$. We conclude that the evolution of the dipole 02 “knows” about the dipole 21. This violates the naive dipole independence at large N_c . The issue is that while dipole 02 contains a polarized gluon at x_2 , it does not carry the large transverse momentum needed for generating dipole 21. It is clear from Fig. 14 that the origin of dipoles 02 and 21 is different topologically too.

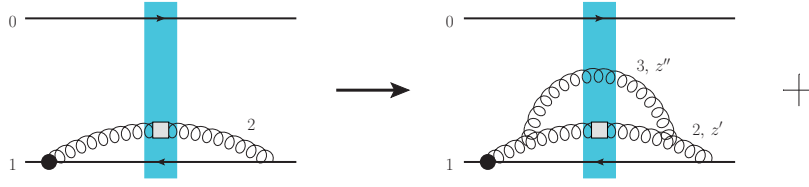


FIG. 14. An illustration of evolution of the neighbor dipole.

To remedy the problem of such neighbor dipole amplitudes, let us write down an evolution equation for $\Gamma_{02,21}(z')$:

$$\Gamma_{02,21}(z') = \Gamma_{02,21}^{(0)}(z') + \frac{\alpha_s N_c}{2\pi^2} \int_{z_i}^{z'} \frac{dz''}{z''} \int_{\rho''^2}^{\min\{x_{02}^2, x_{21}^2 z'/z''\}} \frac{d^2 x_3}{x_{32}^2} [\Gamma_{03,32}(z'') S_{23}(z'') + G_{32}(z'') S_{03}(z'') + G_{23}(z'') S_{03}(z'') - \Gamma_{02,21}(z'')]. \quad (82)$$

Here $\rho''^2 = 1/(z'' s)$. Equation (82) is illustrated diagrammatically in the lower panel of Fig. 13.

Equations (80) and (82) give a coupled closed system of equations which need to be solved to find the energy-dependence of G . We leave the solution of these equations for the future work: it may be that, just like with the evolution considered by BER, only numerical solution of these equations is possible.

Equations (80) and (82) combine DLA evolution of helicity distributions with the LLA evolution of S , akin to Eq. (43) of [67]. Note that in the strict DLA approximation $S = 1$. By keeping S in Eqs. (80) and (82) we are combining the DLA evolution for the polarized dipole operator with the LLA saturation corrections in a single equation. Again strictly-speaking such an approximation is not justified, and only a complete LLA calculation (that is, next-to-leading order (NLO) helicity evolution calculation) would show whether we have the right to keep LLA saturation corrections here. Still we argue that such an NLO calculation is not going to change the operator structure of Eq. (58), and, hence Eq. (58) would probably remain valid, while augmented by the LLA helicity evolution term. Therefore, as was also argued in [67], it is probably justified to mix DLA helicity evolution with the LLA unpolarized evolution in Eqs. (80) and (82). Moreover, if one models the target as a nucleus with atomic number $A \gg 1$, then even in the strict DLA limit one can justify keeping the unpolarized Wilson lines S as a resummation of the multiple rescattering parameter $\alpha_s^2 A^{1/3} \sim 1$ [26].

In the strict DLA limit we can simplify Eqs. (80) and (82) then as follows. The unpolarized dipoles do not have any DLA evolution (in our $\alpha_s \ln^2 s$ resummation parameter). Hence, with the DLA accuracy, we put $S = 1$ obtaining

$$G_{01}(z) = G_{01}^{(0)}(z) + \frac{\alpha_s N_c}{2\pi^2} \int_{z_i}^z \frac{dz'}{z'} \int_{\rho^2} \frac{d^2 x_2}{x_{21}^2} \theta(x_{10} - x_{21}) [\Gamma_{02,21}(z') + 2G_{21}(z') - G_{01}(z')], \quad (83a)$$

$$\Gamma_{02,21}(z') = \Gamma_{02,21}^{(0)}(z') + \frac{\alpha_s N_c}{2\pi^2} \int_{z_i}^{z'} \frac{dz''}{z''} \int_{\rho''^2}^{\min\{x_{02}^2, x_{21}^2 z'/z''\}} \frac{d^2 x_{32}}{x_{32}^2} [\Gamma_{03,32}(z'') + 2G_{23}(z'') - \Gamma_{02,21}(z'')]. \quad (83b)$$

Here we have employed the assumption $G_{21} = G_{12}$ which is valid for a longitudinally polarized target (which possesses no preferred transverse direction, if one neglects transverse gradients of the target density). The solution of the coupled equations (83) would give one the intercept of small- x helicity evolution in the large- N_c limit.

E. Large- N_c & N_f Limit

Consider now the case when both N_c and N_f are comparably large, such that we are keeping powers of $\alpha_s N_c = \text{const} \ll 1$ and $\alpha_s N_f = \text{const}' \ll 1$, while neglecting the subleading powers of $1/N_c$ and $1/N_f$.

In addition to $G_{10}(z)$ defined in Eq. (77) above, which is made out of quark and anti-quark lines of gluons (with x_1 line polarized), let us define

$$A_{10}(z) = \frac{1}{2N_c} \left\langle \left\langle \text{tr} \left[V_{\underline{0}}^{unp} V_{\underline{1}}^{pol \dagger} \right] \right\rangle \right\rangle(z) + \frac{1}{2N_c} \left\langle \left\langle \text{tr} \left[V_{\underline{1}}^{pol} V_{\underline{0}}^{unp \dagger} \right] \right\rangle \right\rangle(z) \quad (84)$$

with x_1 being a true quark or anti-quark polarized line and x_0 being the (anti-)quark line of the gluon, and

$$Q_{10}(z) = \frac{1}{2N_c} \left\langle \left\langle \text{tr} \left[V_{\underline{0}}^{unp} V_{\underline{1}}^{pol \dagger} \right] \right\rangle \right\rangle(z) + \frac{1}{2N_c} \left\langle \left\langle \text{tr} \left[V_{\underline{1}}^{pol} V_{\underline{0}}^{unp \dagger} \right] \right\rangle \right\rangle(z) \quad (85)$$

with both x_0 and x_1 being true quark and anti-quark lines and x_1 polarized. The definition of A is illustrated in Fig. 15.

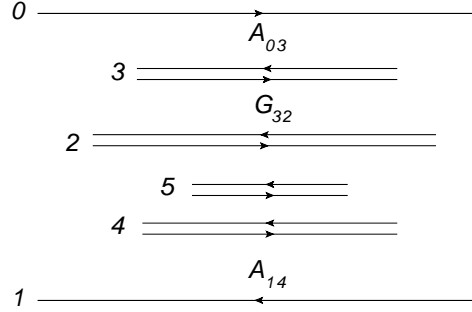


FIG. 15. Different types of dipoles in our large- N_c & N_f resummation. For illustration purposes, any line can be polarized.

An analogue of Eq. (76), but now without neglecting the second term in the curly brackets of Eq. (57), in the large- N_c & N_f limit is

$$\begin{aligned} \frac{1}{N_c} \left\langle \left\langle \text{tr} \left[V_{\underline{0}}^{unp} V_{\underline{1}}^{pol \dagger} \right] \right\rangle \right\rangle(z) &= \frac{1}{N_c} \left\langle \left\langle \text{tr} \left[V_{\underline{0}}^{unp} V_{\underline{1}}^{pol \dagger} \right] \right\rangle \right\rangle_0(z) + \frac{\alpha_s}{2\pi^2} \int_{z_i}^z \frac{dz'}{z'} \int_{\rho'^2} \frac{d^2 x_2}{x_{21}^2} \theta(x_{10} - x_{21}) \\ &\times \left\{ \frac{1}{N_c} \left\langle \left\langle \text{tr} \left[V_{\underline{0}}^{unp} V_{\underline{2}}^{pol \dagger} \right] \right\rangle \right\rangle \left\langle \left\langle \text{tr} \left[V_{\underline{2}}^{unp} V_{\underline{1}}^{unp \dagger} \right] \right\rangle \right\rangle + \frac{1}{N_c} \left\langle \left\langle \text{tr} \left[V_{\underline{0}}^{unp} V_{\underline{2}}^{unp \dagger} \right] \right\rangle \right\rangle \left\langle \left\langle \text{tr} \left[V_{\underline{2}}^{pol} V_{\underline{1}}^{unp \dagger} \right] \right\rangle \right\rangle \right. \\ &+ \frac{1}{N_c} \left\langle \left\langle \text{tr} \left[V_{\underline{0}}^{unp} V_{\underline{2}}^{unp \dagger} \right] \right\rangle \right\rangle \left\langle \left\langle \text{tr} \left[V_{\underline{2}}^{unp} V_{\underline{1}}^{pol \dagger} \right] \right\rangle \right\rangle - \left. \left\langle \left\langle \text{tr} \left[V_{\underline{0}}^{unp} V_{\underline{1}}^{pol \dagger} \right] \right\rangle \right\rangle \right\}(z') \\ &+ \frac{\alpha_s}{4\pi^2} \int_{z_i}^z \frac{dz'}{z'} \int_{\rho'^2} \frac{d^2 x_2}{x_{21}^2} \theta(x_{10}^2 z - x_{21}^2 z') \frac{1}{N_c} \left\langle \left\langle \text{tr} \left[V_{\underline{0}}^{unp} V_{\underline{1}}^{unp \dagger} \right] \right\rangle \right\rangle \left\langle \left\langle \text{tr} \left[V_{\underline{1}}^{unp} V_{\underline{2}}^{pol \dagger} \right] \right\rangle \right\rangle(z'). \end{aligned} \quad (86)$$

Adding a complex conjugate to Eq. (86) and dividing by 2 to get $Q_{10}(z)$ on the left we obtain

$$\begin{aligned} Q_{10}(z) &= Q_{10}^{(0)}(z) + \frac{\alpha_s N_c}{2\pi^2} \int_{z_i}^z \frac{dz'}{z'} \int_{\rho'^2} \frac{d^2 x_2}{x_{21}^2} \theta(x_{10} - x_{21}) \\ &\times [S_{21}(z') \Gamma_{02, 21}(z') + S_{02}(z') G_{21}(z') + S_{02}(z') A_{12}(z') - Q_{10}(z')] \\ &+ \frac{\alpha_s N_c}{4\pi^2} \int_{z_i}^z \frac{dz'}{z'} \int_{\rho'^2} \frac{d^2 x_2}{x_{21}^2} \theta(x_{10}^2 z - x_{21}^2 z') S_{01}(z') A_{21}(z'). \end{aligned} \quad (87)$$

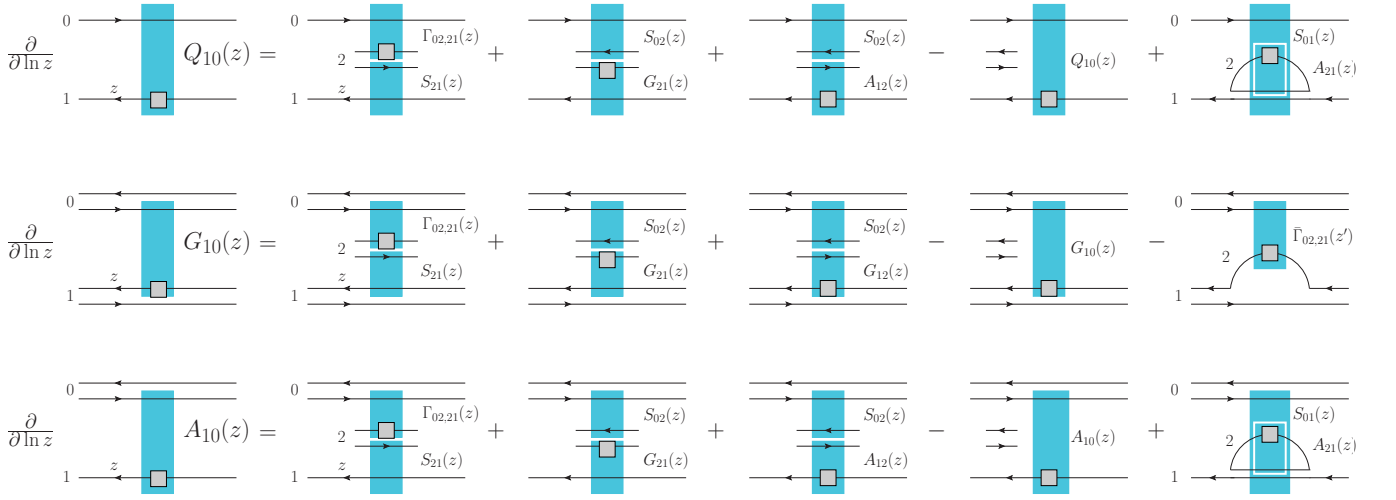


FIG. 16. Large- N_c & N_f helicity evolution for the polarized dipole amplitudes Q , G and A .

Equation (87) is illustrated diagrammatically in the first line of Fig. 16, where again we do not show the initial condition term for simplicity.

Now, we turn to the evolution for $G_{10}(z)$. Adding to Eq. (86) its complex conjugate and dividing by two gives

$$\begin{aligned}
G_{10}(z) &= G_{10}^{(0)}(z) + \frac{\alpha_s N_c}{2\pi^2} \int_{z_i}^z \frac{dz'}{z'} \int \frac{d^2 x_2}{x_{21}^2} \theta(x_{10} - x_{21}) \\
&\times [S_{21}(z') \Gamma_{02,21}(z') + S_{02}(z') G_{21}(z') + S_{02}(z') G_{12}(z') - G_{10}(z')] \\
&- \frac{\alpha_s N_f}{4\pi^2} \int_{z_i}^z \frac{dz'}{z'} \int \frac{d^2 x_2}{x_{21}^2} \theta(x_{10}^2 z - x_{21}^2 z') \bar{\Gamma}_{02,21}(z'), \tag{88}
\end{aligned}$$

where we have “by hand” removed the last term in Eq. (86) as an impossible one in the evolution of a fundamental dipole made out of quark and anti-quark lines of two gluons. We have also added “by hand” the N_f -term arising due to $G \rightarrow q\bar{q}$ splitting. The term comes from the gluon dipole evolution (62) and is illustrated in Fig. 17: one has to take the large- N_c & N_f limit of (62) to obtain this term in Eq. (88). Note a new object, $\bar{\Gamma}_{02,21}$, which is the neighbor dipole amplitude with line 2 being an actual polarized quark (or anti-quark), and, unlike in $\Gamma_{02,21}$, not a quark (or anti-quark) line of a large- N_c gluon. Equation (88) is illustrated diagrammatically in the second line of Fig. 16.

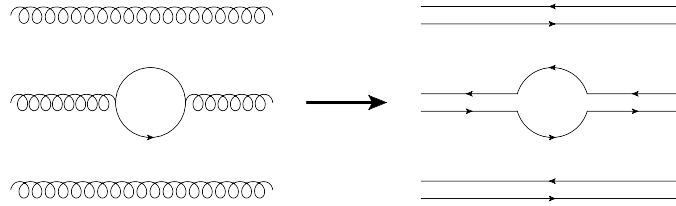


FIG. 17. Diagram illustrating the origin of the last term in Eq. (88).

Finally, the evolution for $A_{01}(z)$ reads

$$\begin{aligned}
A_{10}(z) &= A_{10}^{(0)}(z) + \frac{\alpha_s N_c}{2\pi^2} \int_{z_i}^z \frac{dz'}{z'} \int \frac{d^2 x_2}{x_{21}^2} \theta(x_{10} - x_{21}) \\
&\times [S_{21}(z') \Gamma_{02,21}(z') + S_{02}(z') G_{21}(z') + S_{02}(z') A_{12}(z') - A_{10}(z')] \\
&+ \frac{\alpha_s N_c}{4\pi^2} \int_{z_i}^z \frac{dz'}{z'} \int \frac{d^2 x_2}{x_{21}^2} \theta(x_{10}^2 z - x_{21}^2 z') S_{01}(z') A_{21}(z'), \tag{89}
\end{aligned}$$

as can also be obtained from Eq. (86). It is depicted in the last line of Fig. 16.

Note that Eq. (82) also has to be modified yielding

$$\begin{aligned}
\Gamma_{02,21}(z') &= \Gamma_{02,21}^{(0)}(z') + \frac{\alpha_s N_c}{2\pi} \int_{z_i}^{z'} \frac{dz''}{z''} \int_{\rho'^{1/2}}^{\min\{x_{02}^2, x_{21}^2 z'/z''\}} \frac{dx_{32}^2}{x_{32}^2} \\
&\times [\Gamma_{03,32}(z'') S_{23}(z'') + G_{32}(z'') S_{03}(z'') + G_{23}(z'') S_{03}(z'') - \Gamma_{02,21}(z'')] \\
&- \frac{\alpha_s N_f}{4\pi} \int_{z_i}^{z'} \frac{dz''}{z''} \int_{\rho'^{1/2}}^{x_{21}^2 z'/z''} \frac{dx_{32}^2}{x_{32}^2} \bar{\Gamma}_{03,32}(z').
\end{aligned} \tag{90}$$

We also need an equation for $\bar{\Gamma}$:

$$\begin{aligned}
\bar{\Gamma}_{02,21}(z') &= \bar{\Gamma}_{02,21}^{(0)}(z') + \frac{\alpha_s N_c}{2\pi} \int_{z_i}^{z'} \frac{dz''}{z''} \int_{\rho'^{1/2}}^{\min\{x_{02}^2, x_{21}^2 z'/z''\}} \frac{dx_{32}^2}{x_{32}^2} \\
&\times [\Gamma_{03,32}(z'') S_{23}(z'') + G_{32}(z'') S_{03}(z'') + A_{23}(z'') S_{03}(z'') - \bar{\Gamma}_{02,21}(z'')] \\
&+ \frac{\alpha_s N_c}{4\pi} \int_{z_i}^{z'} \frac{dz''}{z''} \int_{\rho'^{1/2}}^{x_{21}^2 z'/z''} \frac{dx_{32}^2}{x_{32}^2} S_{02}(z') A_{32}(z').
\end{aligned} \tag{91}$$

Both of these equations follow from Eqs. (58) and (62). They are diagrammatically illustrated in Fig. 18.

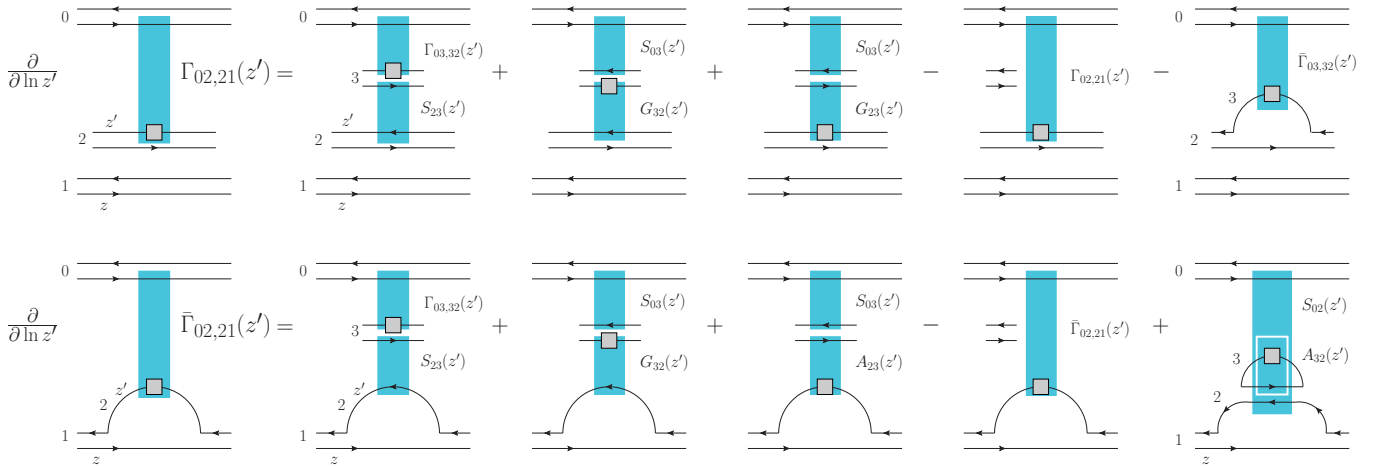


FIG. 18. Large- N_c & N_f helicity evolution for the polarized neighbor dipole amplitudes Γ and $\bar{\Gamma}$.

Equations (87), (88), (89), (90), and (91) are the large- N_c & N_f evolution equations which are DLA in polarization-dependent terms, but also include LLA saturation corrections through the S -matrices. They are the main result of this Subsection.

In the pure DLA limit we linearize all these equations by putting $S = 1$ in them (we again assume that $G_{01} = G_{10}$,

which is true for a large, longitudinally polarized target):

$$\begin{aligned}
Q_{01}(z) &= Q_{01}^{(0)}(z) + \frac{\alpha_s N_c}{2\pi^2} \int_{z_i}^z \frac{dz'}{z'} \int_{\rho^2} \frac{d^2 x_2}{x_{21}^2} \theta(x_{10} - x_{21}) [G_{12}(z') + \Gamma_{02,21}(z') + A_{21}(z') - Q_{01}(z')] \\
&\quad + \frac{\alpha_s N_c}{4\pi^2} \int_{z_i}^z \frac{dz'}{z'} \int_{\rho^2} \frac{d^2 x_2}{x_{21}^2} \theta(x_{10}^2 z - x_{21}^2 z') A_{21}(z'), \tag{92a}
\end{aligned}$$

$$\begin{aligned}
G_{10}(z) &= G_{10}^{(0)}(z) + \frac{\alpha_s N_c}{2\pi^2} \int_{z_i}^z \frac{dz'}{z'} \int_{\rho^2} \frac{d^2 x_2}{x_{21}^2} \theta(x_{10} - x_{21}) [\Gamma_{02,21}(z') + 2 G_{12}(z') - G_{01}(z')] \\
&\quad - \frac{\alpha_s N_f}{4\pi^2} \int_{z_i}^z \frac{dz'}{z'} \int_{\rho^2} \frac{d^2 x_2}{x_{21}^2} \theta(x_{10}^2 z - x_{21}^2 z') \bar{\Gamma}_{02,21}(z'), \tag{92b}
\end{aligned}$$

$$\begin{aligned}
A_{01}(z) &= A_{01}^{(0)}(z) + \frac{\alpha_s N_c}{2\pi^2} \int_{z_i}^z \frac{dz'}{z'} \int_{\rho^2} \frac{d^2 x_2}{x_{21}^2} \theta(x_{10} - x_{21}) [G_{12}(z') + \Gamma_{02,21}(z') + A_{21}(z') - A_{01}(z')] \\
&\quad + \frac{\alpha_s N_c}{4\pi^2} \int_{z_i}^z \frac{dz'}{z'} \int_{\rho^2} \frac{d^2 x_2}{x_{21}^2} \theta(x_{10}^2 z - x_{21}^2 z') A_{12}(z'). \tag{92c}
\end{aligned}$$

The linearized equations for Γ and $\bar{\Gamma}$ in the large- N_c & N_f limit become

$$\begin{aligned}
\Gamma_{02,21}(z') &= \Gamma_{02,21}^{(0)}(z') + \frac{\alpha_s N_c}{2\pi} \int_{z_i}^{z'} \frac{dz''}{z''} \int_{\rho'^2}^{\min\{x_{02}^2, x_{21}^2 z'/z''\}} \frac{dx_{32}^2}{x_{32}^2} [\Gamma_{03,32}(z'') + 2 G_{23}(z'') - \Gamma_{02,21}(z'')] \\
&\quad - \frac{\alpha_s N_f}{4\pi} \int_{z_i}^{z'} \frac{dz''}{z''} \int_{\rho''^2}^{x_{21}^2 z'/z''} \frac{dx_{32}^2}{x_{32}^2} \bar{\Gamma}_{03,32}(z''), \tag{93a}
\end{aligned}$$

$$\begin{aligned}
\bar{\Gamma}_{02,21}(z') &= \bar{\Gamma}_{02,21}^{(0)}(z') + \frac{\alpha_s N_c}{2\pi} \int_{z_i}^{z'} \frac{dz''}{z''} \int_{\rho''^2}^{\min\{x_{02}^2, x_{21}^2 z'/z''\}} \frac{dx_{32}^2}{x_{32}^2} [\Gamma_{03,32}(z'') + G_{23}(z'') + A_{23}(z'') - \bar{\Gamma}_{02,21}(z'')] \\
&\quad + \frac{\alpha_s N_c}{4\pi} \int_{z_i}^{z'} \frac{dz''}{z''} \int_{\rho''^2}^{x_{21}^2 z'/z''} \frac{dx_{32}^2}{x_{32}^2} A_{32}(z''). \tag{93b}
\end{aligned}$$

Clearly in the large- N_c / fixed- N_f limit the linearized equations for $G_{01}(z)$ and $\Gamma_{02,21}(z')$ become a closed system of equations (83) again, as employed in the previous Subsection. Since our final observable, quark helicity TMD or hPDF, is related to Q , for the large- N_c limit to be relevant, G should dominate (or at least be comparable to) A .

The linearized equations (92) and (93), when solved, should yield the helicity evolution intercept in the large- N_c & N_f limit. This number should be compared to the all-orders in N_c & N_f result of BER [1]. Solution of Eqs. (92) and (93) is left for the future (probably numerical) work.

VI. CONCLUSIONS AND OUTLOOK

In this paper we have constructed small- x evolution equations governing the leading x dependence of the fundamental and adjoint polarized dipole operators (47) and (48) given by Eqs. (58) and (62) respectively. The equations resum double logarithms of x (powers of $\alpha_s \ln^2(1/x)$) in helicity evolution, and also include saturation effects through unpolarized dipoles, to be evolved with the LLA BK/JIMWLK evolution (resumming powers of $\alpha_s \ln(1/x)$).

The equations are not closed, but they do become closed in the two limits considered in this work: the large- N_c and the large- N_c & N_f limits. In the large- N_c limit the helicity evolution is given by a closed system of two equations, (80) and (82). In the large- N_c & N_f limit the closed system consists of five equations, (87), (88), (89), (90), and (91).

Solution of these equations, while not straightforward, should be possible in principle, and is left for future work. The polarized quark dipole operator gives us energy dependence of the quark helicity TMD $g_{1L}(x, k_T)$ via Eq. (15) and of the quark hPDF $\Delta q(x, Q^2)$ via Eq. (17). Therefore, it is very important to solve the helicity evolution equations obtained here, in order to evaluate the small- x quark contribution to the helicity sum rule and to address a possible resolution of the spin puzzle.

Indeed higher-order (LLA) corrections to our DLA results need to be calculated as well. While the ladder approximation is only a rough estimate of the result, it is perhaps troubling that for realistic α_s the quark hPDF grows with x faster than the unpolarized structure functions, as one can see from Eq. (74). If this steep growth is also the case with the full DLA solution, it is clear that higher-order LLA corrections must be numerically large for $\alpha_s \approx 0.3$ to reduce the growth of the intercept. It is, therefore, possible that LLA corrections are very important for the present phenomenology.

Another important possible source of the intercept reduction is saturation effects. Indeed saturation effects are defined as a slowdown of an observable's growth with increasing energy or decreasing x . The impact of saturation on the DLA Reggeon evolution, which is similar to our helicity evolution considered here, was studied in [67]. It was shown that indeed saturation effects reduce the Reggeon intercept.

There is another consideration which makes it important to include saturation effects in the problem at hand. In all of the above DLA evolution equations we integrate over x_{21}^2 up to $x_{10}^2 z/z'$. (For definitiveness let us consider Eq. (58).) Since $\Lambda^2/s = z_i < z' < z < 1$ we get the absolute upper bound on the x_{21} integral,

$$x_{21}^2 < x_{10}^2 \frac{z}{z'} < x_{10}^2 \frac{s}{\Lambda^2}. \quad (94)$$

Since $x_{10} \sim 1/k_T$ with k_T the typical transverse momentum in the problem, and $s x_{10}^2 \sim s/k_T^2 \gg 1$, we have

$$x_{10}^2 \frac{s}{\Lambda^2} \gg \frac{1}{\Lambda^2} \quad (95)$$

and the upper bound of the x_{21}^2 -integration may end up in the non-perturbative IR region. Throughout the calculations in this paper we simply assumed that everything is perturbative, and never worried about the transverse coordinate (or momentum) integration regions. However, this is indeed potentially dangerous. While the equations (80) and (82) appear to be insensitive to the deep IR region, Eqs. (87), (88), (89), (90), and (91) need saturation effects to stay IR safe. As usual, saturation effects come in through the unpolarized dipole S -matrices, effectively cutting off the IR regions of integration, and justifying our perturbative approach to the problem. Their impact on the intercept of helicity evolution is likely to be important and needs to be studied in detail in the future.

ACKNOWLEDGMENTS

The authors are grateful to Raju Venugopalan for his support and encouragement throughout the project and a critical reading of the manuscript. The authors would also like to thank Ian Balitsky, Joachim Bartels, Giovanni Chirilli, and Al Mueller for informative discussions. YK would like to thank Andreas Metz and Kirill Tuchin for encouraging him to think about the subject in the course of the past several years. This material is based upon work supported by the U.S. Department of Energy, Office of Science, Office of Nuclear Physics under Award Number de-sc0004286 (YK), the RIKEN BNL Research Center (DP), and DOE Contract No. de-sc0012704 (MS). MS receives additional support from an EIC program development fund from BNL.

Appendix A

Let us calculate the tree-level (Born) quark exchange amplitude contributing to the initial conditions of our evolution equations; for a similar discussion, see Appendix B of [67]. We consider the annihilation amplitude of an antiquark with momentum p_1 and spin σ_1 on a quark with momentum p_2 and spin σ_2 at high energy (Fig. 19). We will treat all particles as massless, and we take p_1 to be moving along the light-cone x^+ axis and p_2 to be moving along the light-cone x^- axis. Let us fix the external momenta to be

$$\begin{aligned} p_1^\mu &= (p_1^+, 0^-, \underline{0}) = (zP^+, 0^-, \underline{0}), \\ p_2^\mu &= (0^+, p_2^-, \underline{0}), \end{aligned} \quad (A1)$$

where z is the longitudinal momentum fraction of the antiquark, with $zs = (p_1 + p_2)^2 = 2zP^+p_2^-$. We also define Sudakov momentum fractions $\alpha \equiv k^+/p_1^+$ and $\beta \equiv |k^-|/p_2^-$ and employ the on-shell conditions for the produced

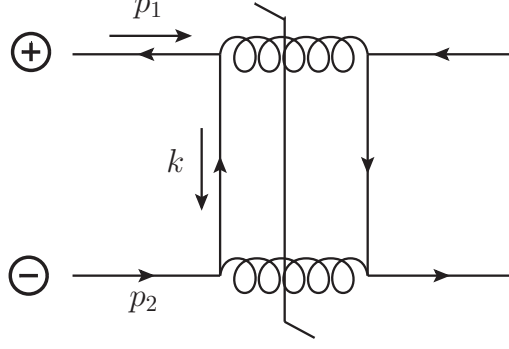


FIG. 19. The tree-level forward Reggeon exchange amplitude.

gluons to write

$$\begin{aligned}
 k^- &= p_1^- - (p_1 - k)^- = -\frac{1}{2} \frac{k_T^2}{(1 - \alpha)p_1^+} \equiv -\beta p_2^-, \\
 k^+ &= (p_2 + k)^+ - p_2^+ = \frac{1}{2} \frac{k_T^2}{(1 - \beta)p_2^-} \equiv \alpha p_1^+.
 \end{aligned} \tag{A2}$$

Regge kinematics corresponds to the limit $k_T^2 \ll zs$ and, therefore, $\alpha \approx \beta \approx k_T^2/(zs) \ll 1$. In this limit one then has $k^2 = -\alpha\beta zs - k_T^2 \approx -k_T^2$.

The $q\bar{q} \rightarrow G\bar{G}$ squared amplitude (averaged over colors of the quark and antiquark and summed over the outgoing gluon spins λ_1, λ_2) is

$$\begin{aligned}
 \langle M^2 \rangle &\equiv \frac{1}{N_c^2} \sum_{\text{colors}} \sum_{\lambda_1, \lambda_2} |M|^2 \\
 &= \frac{C_F^2 g^4}{N_c k_T^4} [\bar{V}_{\sigma_1}(p_1) \gamma_\mu \not{k} \gamma_\nu U_{\sigma_2}(p_2)] [\bar{U}_{\sigma_2}(p_2) \gamma^\nu \not{k} \gamma^\mu V_{\sigma_1}(p_1)],
 \end{aligned} \tag{A3}$$

where U_σ (V_σ) is a quark (antiquark) spinor with spin σ . Rather than computing the spinor products independently, it is convenient to isolate the desired polarizations σ_1, σ_2 using the chirality projectors:

$$[U_\sigma(p)]_\alpha [\bar{U}_\sigma(p)]_\beta \rightarrow [\mathcal{P}_\sigma \not{p}]_{\alpha\beta}, \tag{A4}$$

where

$$\mathcal{P}_\sigma \equiv \frac{1}{2} (1 + \sigma \gamma^5), \tag{A5}$$

which satisfies

$$\begin{aligned}
 \mathcal{P}_\sigma \mathcal{P}_{\sigma'} &= \delta_{\sigma\sigma'} \mathcal{P}_\sigma, \\
 \mathcal{P}_\sigma \gamma^\mu &= \gamma^\mu \mathcal{P}_{-\sigma}.
 \end{aligned} \tag{A6}$$

For V_σ we similarly make the replacement $V_\sigma \bar{V}_\sigma \rightarrow \mathcal{P}_{-\sigma} \not{p}$. Thus $\mathcal{P}_+ = \mathcal{P}_R$ is the right-handed projector and $\mathcal{P}_- = \mathcal{P}_L$ is the left-handed projector. Using this in (A3) gives

$$\begin{aligned}
 \langle M^2 \rangle &= \frac{C_F^2 g^4}{N_c k_T^4} \text{Tr}[\mathcal{P}_{-\sigma_1} \not{p}_1 \gamma_\mu \not{k} \gamma_\nu \mathcal{P}_{\sigma_2} \not{p}_2 \gamma^\nu \not{k} \gamma^\mu] \\
 &= 4 \frac{C_F^2 g^4}{N_c k_T^4} \delta_{-\sigma_1 \sigma_2} \text{Tr}[\mathcal{P}_{-\sigma_1} \not{k} \not{p}_2 \not{k} \not{p}_1] \\
 &= 4(4\pi)^2 \frac{\alpha_s^2 C_F^2}{N_c} \frac{zs}{k_T^2} \delta_{-\sigma_1 \sigma_2}.
 \end{aligned} \tag{A7}$$

The differential cross-section for Reggeon exchange at this order is then

$$\frac{d\sigma_{Reg}^{Born}}{d^2k} = \frac{1}{16\pi^2 z^2 s^2} \langle M^2 \rangle = 4 \frac{\alpha_s^2 C_F^2}{N_c} \frac{1}{zs} \frac{1}{k_T^2} \delta_{-\sigma_1 \sigma_2}, \quad (\text{A8})$$

or written as (the numerator of) a spin asymmetry is

$$\frac{d\Delta\sigma_{Reg}^{Born}}{d^2k} \equiv \frac{1}{2} \left[\frac{d\sigma_{Reg}^{Born}(+, +)}{d^2k} - \frac{d\sigma_{Reg}^{Born}(+, -)}{d^2k} \right] = -2 \frac{\alpha_s^2 C_F^2}{N_c} \frac{1}{zs} \frac{1}{k_T^2}. \quad (\text{A9})$$

We see explicitly that this polarization-dependent interaction is suppressed by one power of zs .

Next, let us calculate the tree-level gluon exchange in Fig. 20. This diagram can also lead to a spin asymmetry if one of the gluons in the squared amplitude is sub-eikonal and spin dependent, as will be seen clearly in what follows. At the level of the $q\bar{q} \rightarrow q\bar{q}$ squared amplitude, we find

$$\langle M^2 \rangle = g^4 \frac{C_F}{2N_c} \frac{1}{(k^2)^2} \text{Tr} \left[\mathcal{P}_{-\sigma_1} \not{p}_1 \gamma^\mu (\not{p}_1 - \not{k}) \gamma^\rho \right] \text{Tr} \left[\mathcal{P}_{\sigma_2} \not{p}_2 \gamma_\rho (\not{p}_2 + \not{k}) \gamma_\mu \right]. \quad (\text{A10})$$

The usual Pomeron exchange keeps the contribution from (A10) that is dominant at high energies, i.e., eikonal gluon

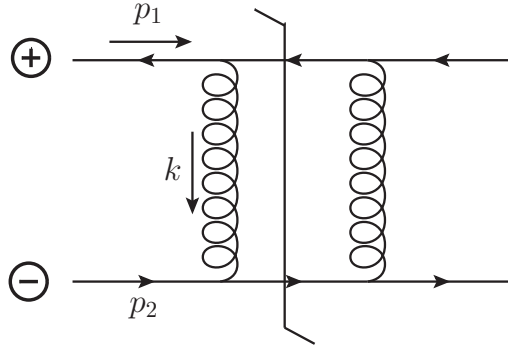


FIG. 20. The tree-level Pomeron exchange.

vertices. This leads to the dominant high-energy scattering cross-section, but is insensitive to the spins σ_1, σ_2 and, therefore, does not contribute to the initial conditions of the helicity evolution. On the other hand, the spin-dependent part of the first trace factor in Eq. (A10) gives

$$-\frac{1}{2} \sigma_1 \text{Tr} \left[\gamma_5 \not{p}_1 \gamma^\mu (\not{p}_1 - \not{k}) \gamma^\rho \right] = \frac{1}{2} \sigma_1 \text{Tr} \left[\gamma_5 \not{p}_1 \gamma^\mu \not{k} \gamma^\rho \right] = -2i \sigma_1 p_1^+ k_\alpha \epsilon^{-\mu\alpha\rho}, \quad (\text{A11})$$

which tells us, because of the antisymmetry of the epsilon tensor, that either μ or ρ must be a transverse index, i.e., one must have a sub-eikonal vertex. In the end we obtain

$$\frac{d\Delta\sigma_{Pom}^{Born}}{d^2k} = \frac{C_F}{N_c} \alpha_s^2 \frac{1}{zs} \frac{1}{k_T^2}, \quad (\text{A12})$$

which is of the same order in the energy zs as the Born diagram for Reggeon exchange given in Eq. (A9).

The initial conditions for our helicity evolution equations can be constructed out of the cross sections Eqs. (A9) and (A12), “dressed” by unpolarized multiple rescatterings [67].

-
- [1] J. Bartels, B. Ermolaev, and M. Ryskin, *Flavor singlet contribution to the structure function $G(1)$ at small x* , *Z.Phys.* **C72** (1996) 627–635, [[hep-ph/9603204](#)].
 - [2] L. V. Gribov, E. M. Levin, and M. G. Ryskin, *Semihard Processes in QCD*, *Phys. Rept.* **100** (1983) 1–150.
 - [3] A. H. Mueller and J.-w. Qiu, *Gluon recombination and shadowing at small values of x* , *Nucl. Phys.* **B268** (1986) 427.
 - [4] L. D. McLerran and R. Venugopalan, *Computing quark and gluon distribution functions for very large nuclei*, *Phys. Rev.* **D49** (1994) 2233–2241, [[hep-ph/9309289](#)].

- [5] L. D. McLerran and R. Venugopalan, *Gluon distribution functions for very large nuclei at small transverse momentum*, *Phys. Rev.* **D49** (1994) 3352–3355, [[hep-ph/9311205](#)].
- [6] L. D. McLerran and R. Venugopalan, *Green's functions in the color field of a large nucleus*, *Phys. Rev.* **D50** (1994) 2225–2233, [[hep-ph/9402335](#)].
- [7] Y. V. Kovchegov, *Non-abelian Weizsäcker-Williams field and a two-dimensional effective color charge density for a very large nucleus*, *Phys. Rev.* **D54** (1996) 5463–5469, [[hep-ph/9605446](#)].
- [8] Y. V. Kovchegov, *Quantum structure of the non-Abelian Weizsäcker-Williams field for a very large nucleus*, *Phys. Rev.* **D55** (1997) 5445–5455, [[hep-ph/9701229](#)].
- [9] J. Jalilian-Marian, A. Kovner, L. D. McLerran, and H. Weigert, *The intrinsic glue distribution at very small x* , *Phys. Rev.* **D55** (1997) 5414–5428, [[hep-ph/9606337](#)].
- [10] A. H. Mueller, *Soft gluons in the infinite momentum wave function and the BFKL pomeron*, *Nucl. Phys.* **B415** (1994) 373–385.
- [11] A. H. Mueller and B. Patel, *Single and double BFKL pomeron exchange and a dipole picture of high-energy hard processes*, *Nucl. Phys.* **B425** (1994) 471–488, [[hep-ph/9403256](#)].
- [12] A. H. Mueller, *Unitarity and the BFKL pomeron*, *Nucl. Phys.* **B437** (1995) 107–126, [[hep-ph/9408245](#)].
- [13] I. Balitsky, *Operator expansion for high-energy scattering*, *Nucl. Phys.* **B463** (1996) 99–160, [[hep-ph/9509348](#)].
- [14] I. Balitsky, *Factorization and high-energy effective action*, *Phys. Rev.* **D60** (1999) 014020, [[hep-ph/9812311](#)].
- [15] Y. V. Kovchegov, *Small- x F_2 structure function of a nucleus including multiple pomeron exchanges*, *Phys. Rev.* **D60** (1999) 034008, [[hep-ph/9901281](#)].
- [16] Y. V. Kovchegov, *Unitarization of the BFKL pomeron on a nucleus*, *Phys. Rev.* **D61** (2000) 074018, [[hep-ph/9905214](#)].
- [17] J. Jalilian-Marian, A. Kovner, and H. Weigert, *The Wilson renormalization group for low x physics: Gluon evolution at finite parton density*, *Phys. Rev.* **D59** (1998) 014015, [[hep-ph/9709432](#)].
- [18] J. Jalilian-Marian, A. Kovner, A. Leonidov, and H. Weigert, *The Wilson renormalization group for low x physics: Towards the high density regime*, *Phys. Rev.* **D59** (1998) 014014, [[hep-ph/9706377](#)].
- [19] E. Iancu, A. Leonidov, and L. D. McLerran, *The renormalization group equation for the color glass condensate*, *Phys. Lett.* **B510** (2001) 133–144.
- [20] E. Iancu, A. Leonidov, and L. D. McLerran, *Nonlinear gluon evolution in the color glass condensate. I*, *Nucl. Phys.* **A692** (2001) 583–645, [[hep-ph/0011241](#)].
- [21] E. Iancu and R. Venugopalan, *The color glass condensate and high energy scattering in QCD*, [hep-ph/0303204](#).
- [22] H. Weigert, *Evolution at small x_{bj} : The Color Glass Condensate*, *Prog. Part. Nucl. Phys.* **55** (2005) 461–565, [[hep-ph/0501087](#)].
- [23] J. Jalilian-Marian and Y. V. Kovchegov, *Saturation physics and deuteron gold collisions at RHIC*, *Prog. Part. Nucl. Phys.* **56** (2006) 104–231, [[hep-ph/0505052](#)].
- [24] F. Gelis, E. Iancu, J. Jalilian-Marian, and R. Venugopalan, *The Color Glass Condensate*, *Ann.Rev.Nucl.Part.Sci.* **60** (2010) 463–489, [[arXiv:1002.0333](#)].
- [25] J. L. Albacete and C. Marquet, *Gluon saturation and initial conditions for relativistic heavy ion collisions*, *Prog.Part.Nucl.Phys.* **76** (2014) 1–42, [[arXiv:1401.4866](#)].
- [26] Y. V. Kovchegov and E. Levin, *Quantum Chromodynamics at High Energy*. Cambridge University Press, 2012.
- [27] D. Boer, A. Dumitru, and A. Hayashigaki, *Single transverse-spin asymmetries in forward pion production at high energy: Incorporating small- x effects in the target*, *Phys.Rev.* **D74** (2006) 074018, [[hep-ph/0609083](#)].
- [28] D. Boer, A. Utermann, and E. Wessels, *The Saturation scale and its x -dependence from Lambda polarization studies*, *Phys.Lett.* **B671** (2009) 91–98, [[arXiv:0811.0998](#)].
- [29] D. Boer and A. Dumitru, *Polarized hyperons from pA scattering in the gluon saturation regime*, *Phys.Lett.* **B556** (2003) 33–40, [[hep-ph/0212260](#)].
- [30] F. Dominguez, J.-W. Qiu, B.-W. Xiao, and F. Yuan, *On the linearly polarized gluon distributions in the color dipole model*, *Phys.Rev.* **D85** (2012) 045003, [[arXiv:1109.6293](#)].
- [31] A. Metz and J. Zhou, *Distribution of linearly polarized gluons inside a large nucleus*, *Phys.Rev.* **D84** (2011) 051503, [[arXiv:1105.1991](#)].
- [32] Y. V. Kovchegov and M. D. Sievert, *A New Mechanism for Generating a Single Transverse Spin Asymmetry*, *Phys.Rev.* **D86** (2012) 034028, [[arXiv:1201.5890](#)].
- [33] A. Mueller, B.-W. Xiao, and F. Yuan, *Sudakov Resummation in Small- x Saturation Formalism*, *Phys.Rev.Lett.* **110** (2013), no. 8 082301, [[arXiv:1210.5792](#)].
- [34] A. Mueller, B.-W. Xiao, and F. Yuan, *Sudakov double logarithms resummation in hard processes in the small- x saturation formalism*, *Phys.Rev.* **D88** (2013), no. 11 114010, [[arXiv:1308.2993](#)].
- [35] Z.-B. Kang and F. Yuan, *Single Spin Asymmetry Scaling in the Forward Rapidity Region at RHIC*, *Phys.Rev.* **D84** (2011) 034019, [[arXiv:1106.1375](#)].
- [36] Z.-B. Kang and B.-W. Xiao, *Sivers asymmetry of Drell-Yan production in small- x regime*, *Phys.Rev.* **D87** (2013) 034038, [[arXiv:1212.4809](#)].
- [37] A. Schäfer and J. Zhou, *Process dependent nuclear k_{\perp} broadening effect*, *Phys.Rev.* **D88** (2013), no. 7 074012, [[arXiv:1305.5042](#)].
- [38] J. Zhou, *Transverse single spin asymmetries at small x and the anomalous magnetic moment*, *Phys.Rev.* **D89** (2014), no. 7 074050, [[arXiv:1308.5912](#)].
- [39] T. Altinoluk, N. Armesto, G. Beuf, M. Martinez, and C. A. Salgado, *Next-to-eikonal corrections in the CGC: gluon production and spin asymmetries in pA collisions*, *JHEP* **07** (2014) 068, [[arXiv:1404.2219](#)].
- [40] Y. V. Kovchegov and M. D. Sievert, *Sivers function in the quasiclassical approximation*, *Phys. Rev.* **D89** (2014), no. 5

- 054035, [arXiv:1310.5028].
- [41] Y. V. Kovchegov and M. D. Sievert, *Calculating TMDs of an Unpolarized Target: Quasi-Classical Approximation and Quantum Evolution*, arXiv:1505.0117.
- [42] I. Balitsky and A. Tarasov, *Evolution of gluon TMD at low and moderate x* , *Int.J.Mod.Phys.Conf.Ser.* **37** (2015) 0058, [arXiv:1411.0714].
- [43] I. Balitsky and A. Tarasov, *Rapidity evolution of gluon TMD from low to moderate x* , *JHEP* **10** (2015) 017, [arXiv:1505.0215].
- [44] A. Tarasov, *Evolution of gluon TMDs from small to moderate x* , in *Proceedings, QCD Evolution Workshop (QCD 2015)*, 2015. arXiv:1510.0693.
- [45] T. Altinoluk, N. Armesto, G. Beuf, and A. Moscoso, *Next-to-next-to-eikonal corrections in the CGC*, arXiv:1505.0140.
- [46] D. Boer, M. G. Echevarria, P. Mulders, and J. Zhou, *Single spin asymmetries from a single Wilson loop*, arXiv:1511.0348.
- [47] J. C. Collins, D. E. Soper, and G. F. Sterman, *Factorization of Hard Processes in QCD*, *Adv.Ser.Direct.High Energy Phys.* **5** (1988) 1–91, [hep-ph/0409313].
- [48] J. C. Collins and D. E. Soper, *Back-To-Back Jets in QCD*, *Nucl.Phys.* **B193** (1981) 381.
- [49] **European Muon** Collaboration, J. Ashman *et. al.*, *A Measurement of the Spin Asymmetry and Determination of the Structure Function $g(1)$ in Deep Inelastic Muon-Proton Scattering*, *Phys. Lett.* **B206** (1988) 364.
- [50] **European Muon** Collaboration, J. Ashman *et. al.*, *An Investigation of the Spin Structure of the Proton in Deep Inelastic Scattering of Polarized Muons on Polarized Protons*, *Nucl. Phys.* **B328** (1989) 1.
- [51] A. Accardi, J. Albacete, M. Anselmino, N. Armesto, E. Aschenauer, *et. al.*, *Electron Ion Collider: The Next QCD Frontier - Understanding the glue that binds us all*, arXiv:1212.1701.
- [52] E. C. Aschenauer *et. al.*, *The RHIC Spin Program: Achievements and Future Opportunities*, arXiv:1304.0079.
- [53] E.-C. Aschenauer *et. al.*, *The RHIC SPIN Program: Achievements and Future Opportunities*, arXiv:1501.0122.
- [54] R. L. Jaffe and A. Manohar, *The $G(1)$ Problem: Fact and Fantasy on the Spin of the Proton*, *Nucl. Phys.* **B337** (1990) 509–546.
- [55] X.-D. Ji, *Gauge-Invariant Decomposition of Nucleon Spin*, *Phys. Rev. Lett.* **78** (1997) 610–613, [hep-ph/9603249].
- [56] X. Ji, X. Xiong, and F. Yuan, *Proton Spin Structure from Measurable Parton Distributions*, *Phys. Rev. Lett.* **109** (2012) 152005, [arXiv:1202.2843].
- [57] D. de Florian, R. Sassot, M. Stratmann, and W. Vogelsang, *Evidence for polarization of gluons in the proton*, *Phys. Rev. Lett.* **113** (2014), no. 1 012001, [arXiv:1404.4293].
- [58] **NNPDF** Collaboration, E. R. Nocera, R. D. Ball, S. Forte, G. Ridolfi, and J. Rojo, *A first unbiased global determination of polarized PDFs and their uncertainties*, *Nucl. Phys.* **B887** (2014) 276–308, [arXiv:1406.5539].
- [59] E. C. Aschenauer, R. Sassot, and M. Stratmann, *Helicity Parton Distributions at a Future Electron-Ion Collider: A Quantitative Appraisal*, *Phys. Rev.* **D86** (2012) 054020, [arXiv:1206.6014].
- [60] R. Kirschner and L. Lipatov, *Double Logarithmic Asymptotics and Regge Singularities of Quark Amplitudes with Flavor Exchange*, *Nucl.Phys.* **B213** (1983) 122–148.
- [61] R. Kirschner, *Reggeon interactions in perturbative QCD*, *Z.Phys.* **C65** (1995) 505–510, [hep-th/9407085].
- [62] R. Kirschner, *Regge asymptotics of scattering with flavor exchange in QCD*, *Z.Phys.* **C67** (1995) 459–466, [hep-th/9404158].
- [63] S. Griffiths and D. Ross, *Studying the perturbative Reggeon*, *Eur.Phys.J.* **C12** (2000) 277–286, [hep-ph/9906550].
- [64] E. A. Kuraev, L. N. Lipatov, and V. S. Fadin, *The Pomernchuk singularity in non-Abelian gauge theories*, *Sov. Phys. JETP* **45** (1977) 199–204.
- [65] I. Balitsky and L. Lipatov, *The Pomernchuk Singularity in Quantum Chromodynamics*, *Sov.J.Nucl.Phys.* **28** (1978) 822–829.
- [66] J. Bartels, B. Ermolaev, and M. Ryskin, *Nonsinglet contributions to the structure function g_1 at small x* , *Z.Phys.* **C70** (1996) 273–280, [hep-ph/9507271].
- [67] K. Itakura, Y. V. Kovchegov, L. McLerran, and D. Teaney, *Baryon stopping and valence quark distribution at small x* , *Nucl. Phys.* **A730** (2004) 160–190, [hep-ph/0305332].
- [68] G. 't Hooft, *A two-dimensional model for mesons*, *Nucl. Phys.* **B75** (1974) 461.
- [69] G. P. Lepage and S. J. Brodsky, *Exclusive processes in perturbative quantum chromodynamics*, *Phys. Rev.* **D22** (1980) 2157.
- [70] S. J. Brodsky, H.-C. Pauli, and S. S. Pinsky, *Quantum chromodynamics and other field theories on the light cone*, *Phys.Rept.* **301** (1998) 299–486, [hep-ph/9705477].
- [71] S. Meissner, A. Metz, and K. Goeke, *Relations between generalized and transverse momentum dependent parton distributions*, *Phys. Rev.* **D76** (2007) 034002, [hep-ph/0703176].
- [72] V. N. Gribov and L. N. Lipatov, *Deep inelastic $e p$ scattering in perturbation theory*, *Sov. J. Nucl. Phys.* **15** (1972) 438–450.
- [73] G. Altarelli and G. Parisi, *Asymptotic Freedom in Parton Language*, *Nucl. Phys.* **B126** (1977) 298.
- [74] Y. L. Dokshitzer, *Calculation of the Structure Functions for Deep Inelastic Scattering and e^+e^- Annihilation by Perturbation Theory in Quantum Chromodynamics*, *Sov. Phys. JETP* **46** (1977) 641–653.
- [75] Z. Chen and A. H. Mueller, *The dipole picture of high-energy scattering, the BFKL equation and many gluon compound states*, *Nucl. Phys.* **B451** (1995) 579–604.
- [76] F. Dominguez, A. Mueller, S. Munier, and B.-W. Xiao, *On the small- x evolution of the color quadrupole and the Weizsäcker-Williams gluon distribution*, *Phys.Lett.* **B705** (2011) 106–111, [arXiv:1108.1752].
- [77] H. Weigert, *Unitarity at small Bjorken x* , *Nucl. Phys.* **A703** (2002) 823–860, [hep-ph/0004044].

- [78] K. Rummukainen and H. Weigert, *Universal features of JIMWLK and BK evolution at small x* , *Nucl. Phys.* **A739** (2004) 183–226, [[hep-ph/0309306](#)].
- [79] B. I. Ermolaev, M. Greco and S. I. Troyan, *Running coupling effects for the singlet structure function $g(1)$ at small x* , *Phys. Lett.* **B579**, 321 (2004), [[hep-ph/0307128](#)].
- [80] E. Gardi, J. Kuokkanen, K. Rummukainen, and H. Weigert, *Running coupling and power corrections in nonlinear evolution at the high-energy limit*, *Nucl. Phys.* **A784** (2007) 282–340, [[hep-ph/0609087](#)].
- [81] I. I. Balitsky, *Quark Contribution to the Small- x Evolution of Color Dipole*, *Phys. Rev. D* **75** (2007) 014001, [[hep-ph/0609105](#)].
- [82] Y. Kovchegov and H. Weigert, *Triumvirate of Running Couplings in Small- x Evolution*, *Nucl. Phys.* **A 784** (2007) 188–226, [[hep-ph/0609090](#)].
- [83] J. L. Albacete and Y. V. Kovchegov, *Solving high energy evolution equation including running coupling corrections*, *Phys. Rev.* **D75** (2007) 125021, [[0704.0612](#)].
- [84] Y. V. Kovchegov, J. Kuokkanen, K. Rummukainen, and H. Weigert, *Subleading- N_c corrections in non-linear small- x evolution*, *Nucl. Phys.* **A823** (2009) 47–82, [[arXiv:0812.3238](#)].